Journal of Medicinal Chemistry

pubs.acs.org/jmc Article

Discovery of ASTX029, A Clinical Candidate Which Modulates the Phosphorylation and Catalytic Activity of ERK1/2

Tom D. Heightman, Valerio Berdini, Luke Bevan, Ildiko M. Buck, Maria G. Carr, Aurélie Courtin, Joseph E. Coyle, James E. H. Day, Charlotte East, Lynsey Fazal, Charlotte M. Griffiths-Jones, Steven Howard, Justyna Kucia-Tran, Vanessa Martins, Sandra Muench, Joanne M. Munck, David Norton, Marc O'Reilly, Nicholas Palmer, Puja Pathuri, Torren M. Peakman, Michael Reader, David C. Rees, Sharna J. Rich, Alpesh Shah, Nicola G. Wallis, Hugh Walton, Nicola E. Wilsher, Alison J.-A. Woolford, Michael Cooke, David Cousin, Stuart Onions, Jonathan Shannon, John Watts, and Christopher W. Murray*

Cite This: *J. Med. Chem.* 2021, 64, 12286–12303 Read Online

ACCESS | Metrics & More | Article Recommendations | Supporting Information

ABSTRACT: Aberrant activation of the mitogen-activated protein kinase pathway frequently drives tumor growth, and the ERK1/2 kinases are positioned at a key node in this pathway, making them important targets for therapeutic intervention. Recently, a number of ERK1/2 inhibitors have been advanced to investigational clinical trials in patients with activating mutations in B-Raf proto-oncogene or Ras. Here, we describe the discovery of the clinical candidate ASTX029 (**15**) through structure-guided optimization of our previously published isoindolinone lead (**7**). The medicinal chemistry campaign focused on addressing CYP3A4-mediated metabolism and maintaining favorable physicochemical properties. These efforts led to the identification of ASTX029, which showed the desired pharmacological profile combining ERK1/2 inhibition with suppression of phospho-ERK1/2 (pERK) levels, and in addition, it possesses suitable preclinical pharmacokinetic properties predictive of once daily dosing in humans. ASTX029 is currently in a phase I–II clinical trial in patients with advanced solid tumors.

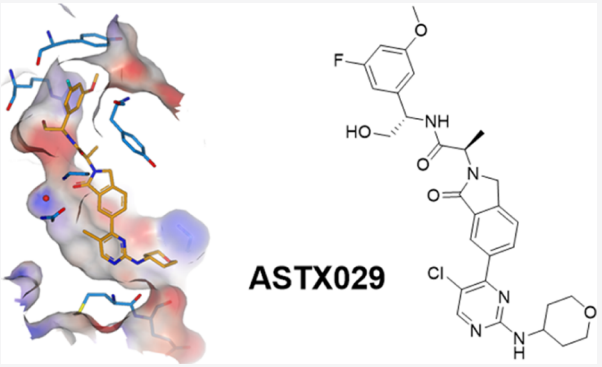

INTRODUCTION

Activation of the Ras-RAF-MEK-ERK signaling pathway (mitogen-activated protein kinase (MAPK) pathway) is one of the major mechanisms driving tumor growth, occurring through activating mutations in upstream growth factor receptors, in the GTPase Ras, or in RAF kinases.[1] Activation of RAF by these mechanisms triggers phosphorylation of MEK1 and 2, which in turn phosphorylates the activation loop of the extracellular related kinases ERK1 and 2 (also known as mitogen activated protein kinases MAPK1 and 2) on the threonine and tyrosine residues in a TEY motif.[2] Activation of ERK1 and 2 leads to not only phosphorylation of substrates in the cytoplasm such as ribosomal S6 kinase (RSK) but also promotes nuclear translocation leading to activation of transcription factors regulating expression of numerous genes involved in cell cycle progression.[3] The ERK1/2 kinases hence form a particularly important node in the signaling pathway and are subject to tight regulation through negative feedback mechanisms including direct inhibitory phosphorylation of upstream pathway proteins and upregulation of expression of MAP kinase phosphatases (DUSPs).[4]

Anticancer drugs targeting the MAPK pathway have shown promising success, including inhibitors of B-Raf proto-oncogene (BRAF) and mitogen activated protein kinase (MEK) which are approved for mutant BRAF melanomas.[5,6] However, the breadth and duration of efficacy of these agents are limited through both innate and drug-induced resistance mechanisms that release negative feedback loops to increase activation of ERK1/2.[7] This has provided strong motivation to seek selective ERK1/2 inhibitors which might show improved efficacy alone or in combination with agents targeting other pathway components.

Received: May 19, 2021
Published: August 13, 2021

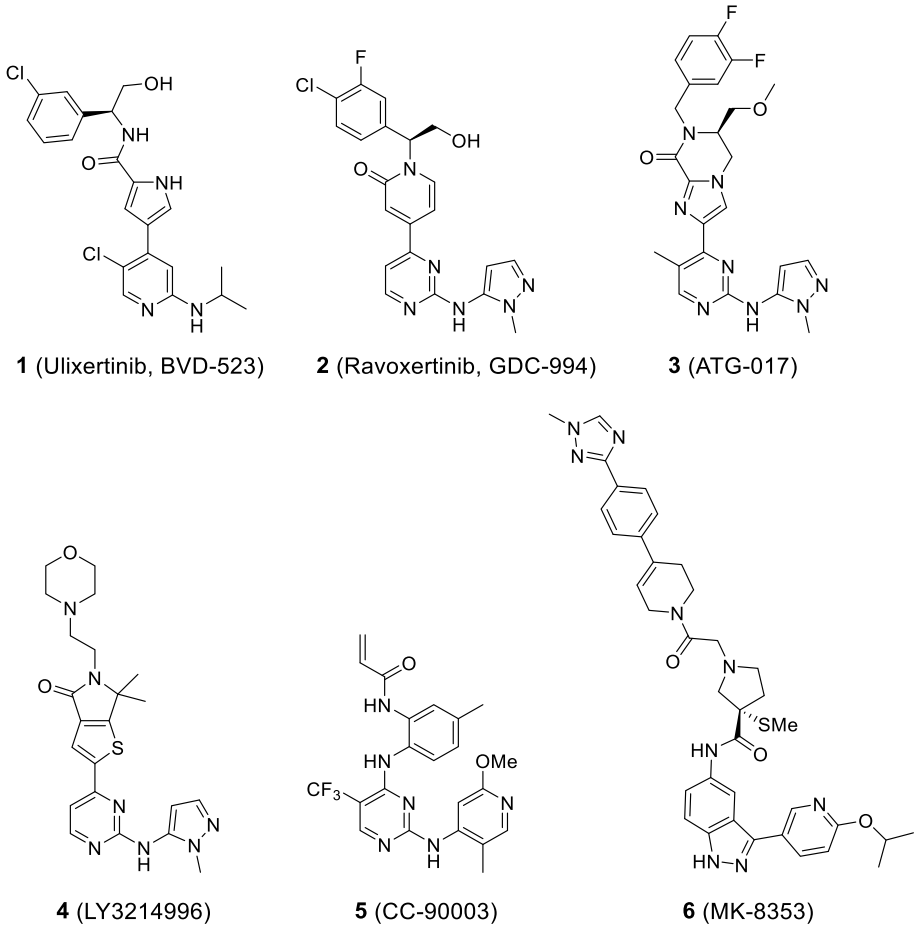

Figure 1. ERK1/2 inhibitors in clinical trials with published structures.

The last decade has seen the development of a variety of ERK1/2 inhibitors with promising preclinical efficacy that have been progressed into clinical trials.[8] Those with disclosed structures (Figure 1) include ulixertinib (BVD-523, **1**),[9] ravoxertinib (GDC-0994, **2**),[10] ATG-017[11] (also known as AZD0364,[12] **3**), and LY3214996 (**4**),[13] which are classical type 1 inhibitors of ERK1/2 catalytic activity; CC-90003 (**5**),[14] which is type 1 covalent inhibitor; and MK-8353 (**6**),[15] which not only inhibits ERK catalytic activity but also profoundly suppresses ERK1/2 phosphorylation by MEK. Additional clinical compounds include KO-947,[16] LTT462,[17] ASN007,[18] and HH2710[19] for which structures are yet to be disclosed.

We and others hypothesized that inhibitors with a dual-mechanism blocking phosphorylation of ERK1/2 and its catalytic activity might have potential to show greater efficacy than type 1 inhibitors, especially in cells with more strongly activated negative pathway loops such as BRAF or MEK inhibitor-resistant mutant BRAF cells and mutant Ras cells.[20] We recently described the fragment-based discovery of the isoindolinone lead **7** (Table 1, compound **27** in ref 21), representing a novel series of ERK1/2 inhibitors with promising oral pharmacokinetics and showing dual inhibition of ERK1/2 catalytic activity and its activation through phosphorylation by MEK. In this paper, we disclose our lead optimization strategy, focusing on enhancing the predicted pharmacokinetics in humans and culminating in the discovery of the clinical candidate ASTX029 (compound **15**). Detailed pharmacological profiling of ASTX029 has been published elsewhere.[22]

RESULTS AND DISCUSSION

Metabolic Studies on the Lead Compound. In the preceding paper, we characterized the lead **7** as a highly potent and selective inhibitor of ERK kinase activity and a modulator of ERK phosphorylation (pERK), with an IC_{50} of 3.5 nM versus pRSK and 2.3 nM versus pERK in A375 cells.[21] Compound **7** showed promising pharmacokinetics in mice, with low *in vivo* clearance of 13.2 mL/min/kg and oral bioavailability of 59%, which translated to efficacy in mutant BRAF Colo205 xenograft studies at either 50 mg/kg once daily or 25 mg/kg twice daily. However, despite this promising profile, detailed metabolic studies demonstrated oxidative metabolism of compound **7** mediated by CYP3A4 with a short *in vitro* half-life (<5 min). We considered this result to present a potential risk of first pass metabolism, limiting oral exposure in humans.[23] Identification of metabolites of compound **7** present in rat bile using LC/MS/MS indicated significant levels of oxidative metabolism at both ends of the molecule, on the tolyl methyl group and the oxan (THP) ring (data not shown). An optimization strategy was therefore set, making changes to reduce the metabolism by directly blocking the vulnerable sites with replacement for more stable isosteres, by conformational rigidification, and by modulating the overall physicochemical properties of the compounds. *In vitro* assays used in the screening cascade are described in the Experimental Procedures section and included an ERK2 biochemical assay (time-resolved fluorescence, TRF), anti-proliferative cellular assays (BRAF mutant A375 and/or

https://doi.org/10.1021/acs.jmedchem.1c00905
J. Med. Chem. 2021, 64, 12286−12303

Table 1. Biochemical and Cellular SARs for Benzylamine Analogues in the Benzolactam ERK1/2 Inhibitor Series

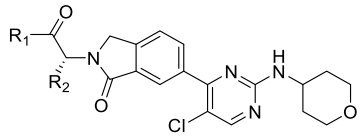

Compound	R1	R2	ERK2 IC_{50} / nM (n)	Prolifn IC_{50} / nM (n)		$T_{1/2}$ / min		
				A375	Colo205	Mic mur	Mic hum	CYP3A4
7	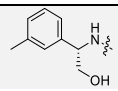	Me	3.0 (2)	4.9 (8)	7.5 (3)	31	12	5.1
8	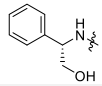	H	49% @ 1 (3)	38 (3)	49 (4)	65	40	10
9		H	2.6 (2)	32 (1)	-	20	10	-
10	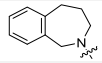	H	14 (2)	330 (2)	-	<5	<5	-
11	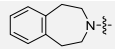	H	5.8 (2)	2500 (3)	-	28	17	28
12	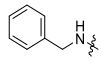	H	26 (3)	45 (4)	73 (3)	65	32	-
13	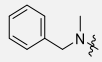	H	25 (3)	48% @ 3000 (1)	-	-	-	-
14	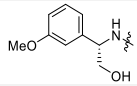	Me	1.3 (6)	5.3 (3)	4.2 (4)	100	27	5.5
15	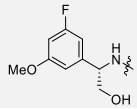	Me	2.7 (3)	3.4 (8)	3.6 (3)	46	33	35
16	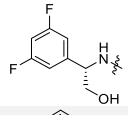	Me	43% @1 (1)	15 (3)	-	49	23	<5
17	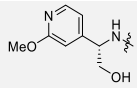	Me	1.8 (4)	18 (6)	27 (2)	120	33	15
18	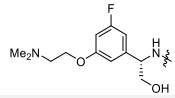	Me	63% @3 (1)	120 (1)	-	-	60	10
19	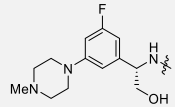	Me	1.8 (1)	18 (2)	-	-	51	-
20	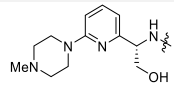	Me	3.1 (2)	12 (5)	-	120	36	17
21	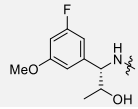	H	35% @1 (1)	2.9 (6)	-	32	25	<5

Colo205 cells), microsomal intrinsic clearance (mouse and human), and CYP3A4 phenotyping, together with physiochemical assays including $ChromLogD_{7.4}$ and kinetic solubility (NMR). Selected compounds were also assessed for pRSK and pERK IC_{50}s (mesoscale discovery (MSD) and ELISA assays in A375 cells, respectively), low-dose mouse PK, PD, and efficacy studies.

Structure–Activity Relationship Studies to Modulate the Metabolic Profile. Structure-based drug design can be used to narrow down the number of plausible options in lead

https://doi.org/10.1021/acs.jmedchem.1c00905
J. Med. Chem. 2021, 64, 12286–12303

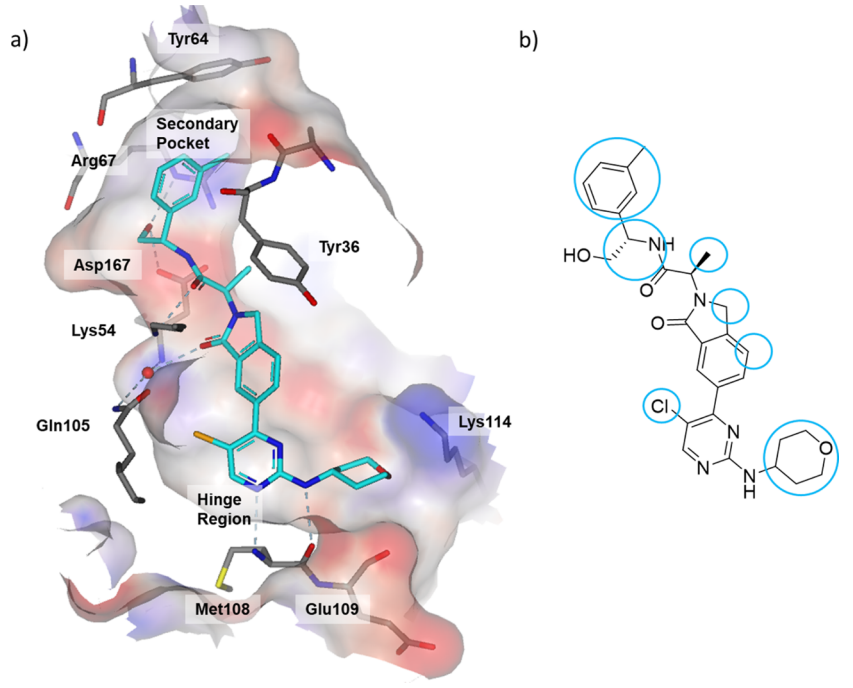

Figure 2. (a) X-ray crystal structure of lead compound **7** in complex with ERK2 (PDB code: 6G9N). Filling both the secondary pocket (upper part of the figure) and the hinge region (lower part of the figure) was believed to be important for the desired pharmacology. (b) Chemical structure of compound **7** indicating potential sites for chemical modification that might modulate the metabolic profile without affecting the binding mode.

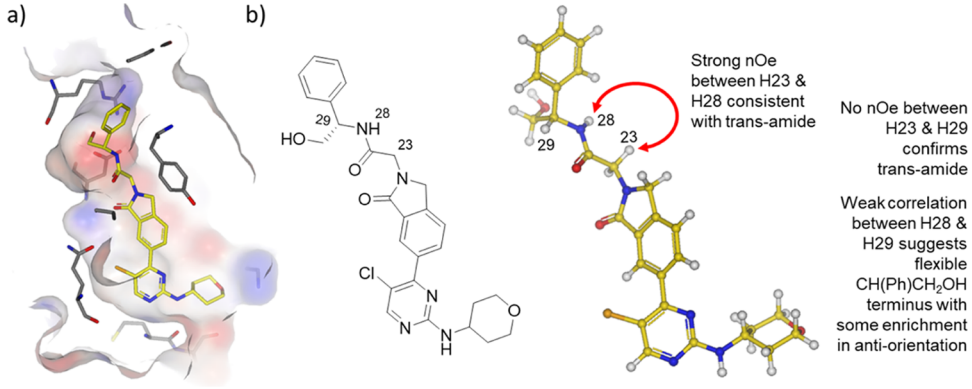

Figure 3. X-ray bound (PDB code: 6G9K) and solution conformations of the unsubstituted phenyl analogue **8**.

optimization, and the crystal structure of the lead **7** in complex with ERK2 showed a number of potential sites for chemical modification to modulate the metabolic profile, while maintaining potency (Figure 2). For example, the metabolic studies discussed above suggested replacements of the oxan ring. The metabolic studies also motivated modifications to the tolyl group by alternative substitutions of the ring and heteroatom insertion or annulation of the secondary amide and/or benzylic carbon. Additionally, the overall lipophilicity of the molecule could be modified by substitution of the acetamide linker or replacement of the chlorine substituent on the aminopyrimidine. Finally, it was hypothesized that the isoindoline might prove to be a metabolic soft spot, so substitution or heteroatom insertion to the 3- or 4-positions of the isoindoline core was explored.

A key element in the optimization strategy was the desire to keep the molecular weight of analogues to a minimum. As described previously, our hypothesis was that occupation of both the hinge region and the secondary pocket (Figure 2a) was required to elicit the desired dual pharmacological profile. This approach necessarily drives toward inhibitors with molecular weight in excess of 500 Da, creating challenges in achieving suitable physicochemical properties for good oral exposure. Hence, before embarking on broad-ranging substituent structure−activity relationship (SAR) studies, we explored whether there might be opportunities for conformational rigidification of the series in order to make potency gains without significant addition of molecular weight. Detailed NMR and computational studies on the unsubstituted analogue **8** suggested a largely extended conformation that was similar to the X-ray bound conformation (Figure 3). The acetamide linker showed a dominant preference for a trans conformation in solution, evidenced by a strong NOE between CH_2(23) and NH(28). However, the weak NOE correlation between NH(28) and the benzylic CH(29) and J−J couplings of ∼6 Hz suggested that the hydroxymethylbenzyl region of **8** underwent more or less free rotation in solution. This prompted us to explore rigidification of this part of the

https://doi.org/10.1021/acs.jmedchem.1c00905
J. Med. Chem. 2021, 64, 12286−12303

molecule, guided by the X-ray crystal structures of the ERK2 complexes with compounds **7** and **8**. Among the approaches attempted, annulating the benzylic carbon to the phenyl ring at the relative ortho-position to give the indane **9** was well tolerated in terms of potency (Table 1). An overlay of the crystal structure of the ERK2 complex of **9** with that of **8** showed an almost identical bound conformation, ratifying the design (Figure 4b); however, the indane **9** showed no benefit

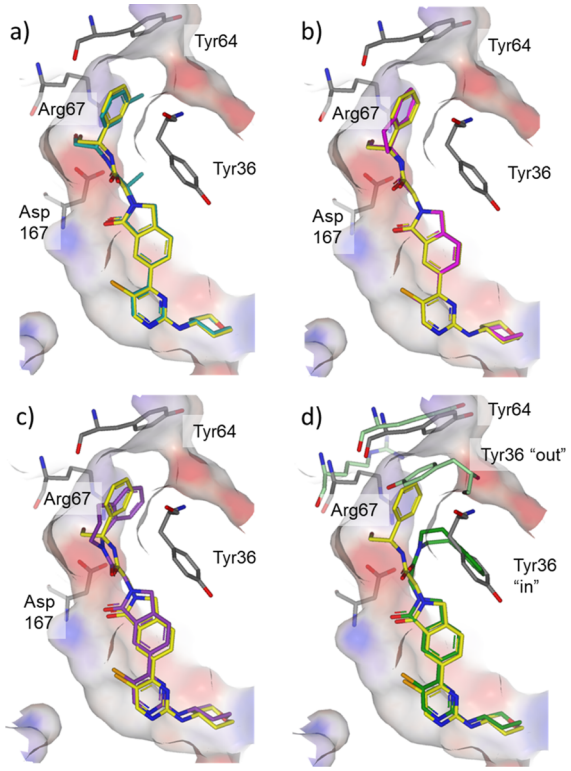

Figure 4. ERK2 costructure of **8** (yellow, PDB code: 6G9K) overlaid with costructures of related conformationally constrained analogues. (a) Lead **7** (cyan, PDB code: 6G9N) shows a minimal change with the addition of Me to the acetyl linker. (b) Indane **9** (magenta) shows a similar bound conformation despite the potential clash between the methylene of the indane ring and the carbonyl of the linker. (c) Asymmetric benzazepine **10** (purple) also shows a similar bound conformation with a minor rearrangement of Arg67 to accommodate loss of the NH and OH. (d) Symmetrical benzazepine **11** (green) shows a different bound conformation in which the fused phenyl ring folds over the isoindoline and mimics Tyr36 in its "in" conformation, while Tyr36 adopts an "out" conformation occupying a similar position to the phenyl of **8**.

in terms of metabolic stability, and hence, the additional synthetic complexity to explore further indane analogues was not warranted. An alternative annulation involved linking the terminal phenyl ring to the amide nitrogen to give the isomeric benzazepines **10** and **11**. Previous SAR had shown that methylation of the amide nitrogen reduced potency in cells (matched pair compounds **12** and **13**, Table 1), and indeed, both benzazepines were less potent in cells than their simpler benzylamine counterpart, compound **12**. Notably, while **10** adopted a similar bound conformation to **8** (Figure 4c), the symmetrical benzazepine isomer **11** bound to ERK2 in a folded conformation, in which the phenyl ring of the benzazepine moiety occupied a similar position to the "in" conformation of Tyr36, while Tyr36 moved into the undesired "out" conformation (Figure 4d).

Next, we explored the effects of substitution and/or heteroatom insertion to the terminal phenyl of compound **7**. As mentioned above, metabolic studies identified the methyl group as a potential site of oxidative metabolism. Replacement of the methyl group with methoxy (compound **14**) was tolerated in terms of potency but gave no advantage in metabolic stability in the CYP3A4 assay (Table 1). The crystal structure of the **14**-ERK2 complex showed space for a small substituent in the 5-position such as a fluoro, leading to the design of compound **15**. Potency was maintained in this 3,5-disubstituted analogue, as well as observing improved CYP3A4 metabolic stability, with a half-life of 35 min (Table 1). The crystal structure of the **15**-ERK2 complex[22] confirmed the designed binding mode, in which the methoxy group contacted the aryl side chain of Tyr64 and the fluoro group occupied a small space between methylenes in the side chains of Tyr64 and Arg67, forming a close contact (2.9 Å) with the hydroxyl side chain of Thr68 (Figure 5a). A wide range of additional monosubstituted and disubstituted analogues were also prepared, but generally showed less promising stability in the CYP3A4 assay, exemplified by the 3,5-difluoro analogue **16** with a half-life of less than 5 min. Incorporation of a heteroatom was tolerated, as exemplified by the methoxypyridine **17**, which showed a potency of 18 nM in A375 cells and a modest half-life of 15 min in the CYP3A4 assay. The crystal structure of the **17**-ERK2 complex showed a similar binding mode to **16**, although Tyr64 shifted away from the methoxypyridine ring presumably to avoid an unfavorable interaction between the nitrogen lone pair of **17** and the electron-rich pi system of Tyr64 (Figure 5b). Noting that the 3-position of this terminal aryl ring provided a vector toward the solvent, we finally explored the effects of appending basic groups to modulate physicochemical properties. Attachment of a dimethylaminoethoxy group to the ring (compound **18**) attenuated the cellular potency while bringing no advantage in terms of metabolic stability (Table 1). The phenylpiperazine **19** and pyridylpiperazine **20** both showed promising activity in cells and were progressed into *in vivo* PK studies (see below). The crystal structure of compound **20** (Figure 5c) confirmed the design hypothesis with the piperazine being accommodated in the ERK protein with minimal disruption to the binding mode.

Overall, from the SAR exploration of the terminal aryl group, the 3-fluoro-5-methoxy derivative demonstrated the most favorable balance of cellular potency and metabolic stability, and this group was therefore used to probe changes in other parts of the molecule.

Inspection of the crystal structure of the **15**-ERK2 complex (Figure 5a) suggested a small space that might accommodate an additional methyl group on the alpha carbon of the alcohol. Hence, the secondary alcohol **21** was designed in which it was anticipated that this additional methyl group might block potential metabolism of the hydroxy group. In the event, **21** showed similar potency to **15** but demonstrated higher CYP3A4-mediated metabolism (Table 1).

The SAR for replacements of the oxan group is summarized in Table 2. A range of other groups were also tolerated if a hydrogen-bond acceptor was suitably positioned to interact with Lys114. The oxetane **22** showed a reasonable balance of cellular activity and metabolic stability. Among the aromatic heterocycles explored, the methylpyrazole **23** showed slightly

https://doi.org/10.1021/acs.jmedchem.1c00905
J. Med. Chem. 2021, 64, 12286−12303

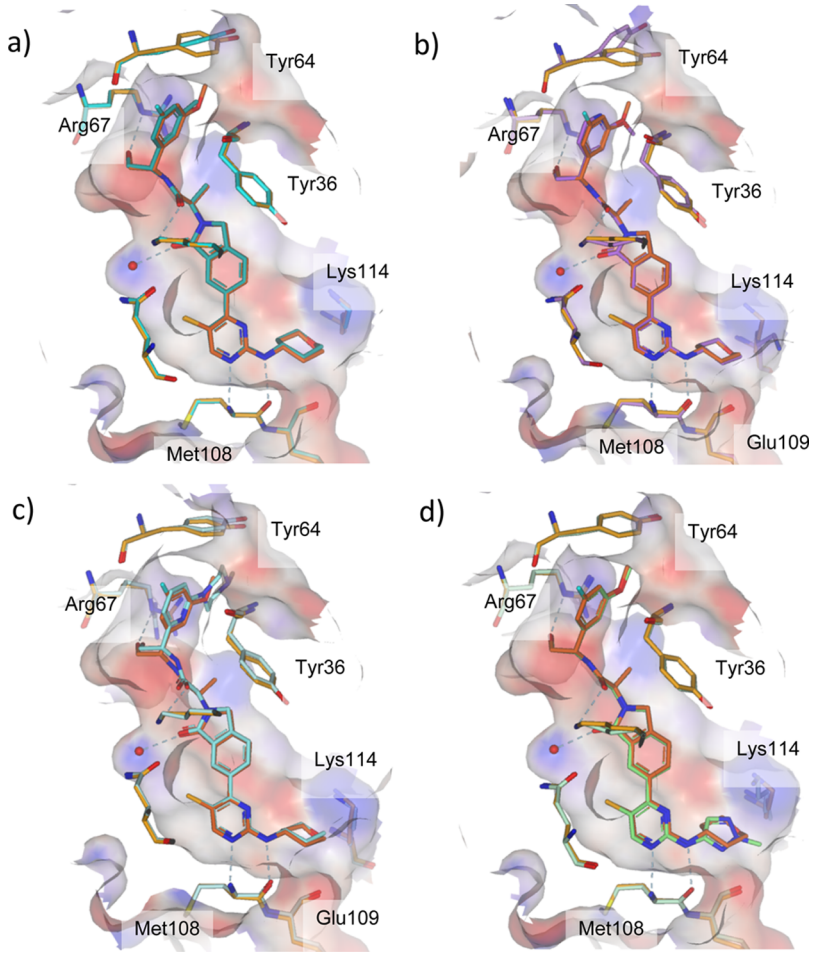

Figure 5. Compound **15** (orange) ERK2 costructure (PDB code: 7AUV) overlaid with costructures of related analogues. (a) Lead **7** (cyan, PDB code: 6G9N), showing minimal changes apart from slight adjustment of Tyr64 reflecting additional contacts. (b) Methoxypyridine **17** (light purple) shows a very similar structure: Tyr64 is pushed away from the pyridyl lone pair and the MeO changes conformation to fill the resulting space. (c) Piperazine analogue **20** (light blue) shows almost identical binding, with additional contacts between the hydrophobic edge of the piperidine ring and the π-system of Tyr64. (d) Triazole **24** (light green) adopts a similar binding mode to **15**, with slight adjustment of Lys114 to allow hydrogen bonding to the triazole N.

weaker activity and was less stable, while the isosteric 2-methyl 1,2,3-triazole and 3-methoxy-4-pyridyl analogues **24** and **25** both showed promising potency and stability. Smaller acyclic groups were also tolerated in this position, such as the hydroxy isopropyl **26**, which possessed promising *in vitro* properties. The crystal structures for one of the better analogues, **24**, showed the expected interactions with minor movements of Lys114 to facilitate hydrogen bonding (Figure 5d). Overall, these oxan replacements provided a range of compounds for study *in vivo*, although it was apparent that none were as potent nor appeared to provide a significant advantage over **15** in terms of metabolic stability.

Finally, we explored smaller changes in the core of **15** (Table 3), guided by the crystal structure of its complex with ERK2 (Figure 5a). The analogue **27** lacking the chloro group on the aminopyrimidine ring was ~6-fold less potent in cells, in keeping with initial findings during the fragment optimization stage,[21] while metabolic stability was similar to **15**. The aza analogue **28** was designed to reduce lipophilicity, positioning the nitrogen lone pair facing toward the solvent to avoid impairing binding to the protein. Compound **28** was slightly weaker than **15** in cellular assays, possibly due to the increase in polar surface area which might compromise permeability. In addition, the reduction in lipophilicity (ChromLogD$_{7.4}$ values **28**: 3.18 cf. **15**: 3.75) did not elicit an increase in human metabolic stability. The analogue **29** was designed with a methyl to block potential metabolism at the isoindolinone 3-position; the structure of the **15**-ERK2 complex suggested that positioning this methyl in the (*S*)-configuration should be sterically accommodated by the protein, while the methyl on the acetamide linker was removed to avoid an intramolecular clash. The design was ratified by good cellular potency; however, this analogue was less metabolically stable than **15** in the CYP3A4 assay. The analogue **30** explored the effect of removing the acetamide methyl and led to a compound with a similar *in vitro* profile to **15**, suitable for further characterization.

***In Vivo* Pharmacokinetics.** During the optimization phase, *in vivo* mouse pharmacokinetic data were collected on a range of compounds (data not shown), and the lipophilicity range for achieving good oral exposure was assessed. As mentioned above, the targeted pharmacological profile necessitated molecular weights in excess of 500, and we, like others,[24] found that relatively high lipophilicity was required to achieve good permeability as reflected in the cell-based assays and in the oral exposure. This however needed to be controlled

https://doi.org/10.1021/acs.jmedchem.1c00905
J. Med. Chem. 2021, 64, 12286−12303

Table 2. Biochemical and Cellular SARs for Oxan Replacements in the Benzolactam ERK1/2 Inhibitor Series

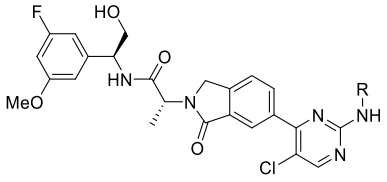

Compound	R1	ERK2 IC_{50} / nM (n)	Prolifn IC_{50} / nM (n)		$T_{1/2}$ / min		
			A375	Colo205	Mic mur	Mic hum	CYP3A4
15		2.7 (3)	3.4 (8)	3.6 (3)	46	35	35
22		49% @ 1 (3)	12 (2)	12 (2)	-	29	50
23		68% @ 3 (2)	29 (2)	10 (2)	35	23	13
24		2.0 (2)	11 (2)	15 (2)	26	26	19
25	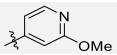	3.5 (3)	11 (3)	-	31	25	27
26		12 (1)	20 (2)	-	-	28	29

Table 3. Biochemical and Cellular SARs for Changes to the Core in the Benzolactam ERK1/2 Inhibitor Series

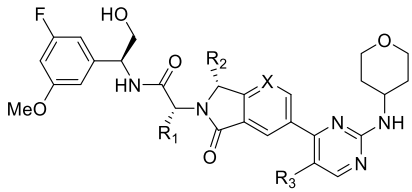

Compound	R1	R2	R3	X	ERK2 IC_{50}/nM (*n*)	prolifn IC_{50}/nM (*n*)		$T_{1/2}$/min		
						A375	Colo205	Mic mur	Mic hum	CYP3A4
15	Me	H	Cl	CH	2.7 (3)	3.4 (8)	3.6 (3)	46	35	35
27	Me	H	H	CH	1.8 (2)	21 (2)	15 (2)		62	49
28	Me	H	Cl	N	2.8 (2)	12 (2)	8 (2)		36	23
29	H	Me	Cl	CH	1.1 (1)	5.9 (2)			22	7.3
30	H	H	Cl	CH	1.1 (3)	4.0 (2)		86	31	

because higher lipophilicity is often associated with general trends for poorer metabolic stability, poorer solubility, and an increased likelihood for off-target effects such as hERG activity. Overall, our analysis suggested that $ChromLogD_{7.4}$ values in the range 3−4 were more likely to lead to favorable property profiles. This empirical observation was used prospectively to model combinations of modifications across the molecule such that only those predicted to be in the desired lipophilicity range were selected for synthesis.

Pharmacokinetics parameters for an illustrative selection of compounds are summarized in Table 4. Both the cyclized derivatives, indane **9** and benzazepine **11**, showed reduced levels of oral exposure compared with the lead **7** and the comparator unsubstituted phenyl analogue **8**. The fluoro-methoxy analogue **15** showed good oral exposure, as did the methoxypyridine **17**; this latter compound showed significantly reduced clearance *in vivo*, potentially due to the metabolic stabilization in this region of the molecule. The fluorophenyl piperazine **19** showed negligible oral exposure, driven by high clearance. The pyridyl piperazine **20** fared better, with lower clearance and an AUC similar to **15**, although surprisingly the volume of distribution of this compound was not increased despite the weakly basic character of the compound.

Oral exposures for the oxan replacements **22**−**26** were comparable to compound **15**, although somewhat lower for the methylpyrazole **23** and hydroxypropyl **26**. The oxetane **22**, triazole **24**, and methoxypyridine **25** showed lower clearance which was reflected in higher exposures.

The analogue **27** lacking the chlorine substituent on the aminopyrimidine showed significantly lower oral exposure and bioavailability compared with its matched pair **15**. The aza-derivative **28** also showed higher clearance and lower oral exposure compared with **15**, somewhat surprising, given its lower lipophilicity. Finally, the analogue of **15** lacking the methyl substitution on the acetamide linker, compound **30**, also showed significantly higher clearance reflected in lower oral exposure, consistent with previous observations suggesting that this substitution stabilizes this part of the molecule to metabolism.[21]

https://doi.org/10.1021/acs.jmedchem.1c00905
J. Med. Chem. 2021, 64, 12286−12303

Table 4. *In Vitro* and *In Vivo* Pharmacokinetic Parameters for Selected Compounds[a]

		i.v.		p.o.		
Compound	ChromLogD$_{7.4}$	Cl (mL/min/kg)	V_{dss} (L/kg)	AUC (ng h/mL)	$T_{1/2}$ (h)	F (%)
7	3.9	13	0.6	3700	0.8	59
8	3.0	11	0.55	3000	2.5	41
9	3.6	35	0.91	960	0.89	40
11	4.7	19	0.45	440	1.4	10
15	3.8	22	0.68	1600	2.9	42
17	3.0	6.8	0.26	2400	1.5	20
19	3.6	124	3.8	18	nd	nd
20	3.3	8.7	0.76	1300	1.0	15
22	3.3	9.4	0.71	2647	1.7	30
23	3.3	13	0.52	824	1.1	13
24	3.7	8.3	0.46	6400	1.5	64
25	4.2	4.6	0.56	4100	1.0	23
26	3.1	23	1.4	310	1.8	9
27	3.2	17	1.0	320	1.2	7
28	3.2	37	1.9	500	1.9	23
30	3.3	54	1.4	150	1.5	10

[a]Mice were administered a single 0.5 mg/kg dose intravenously or 5 mg/kg orally.

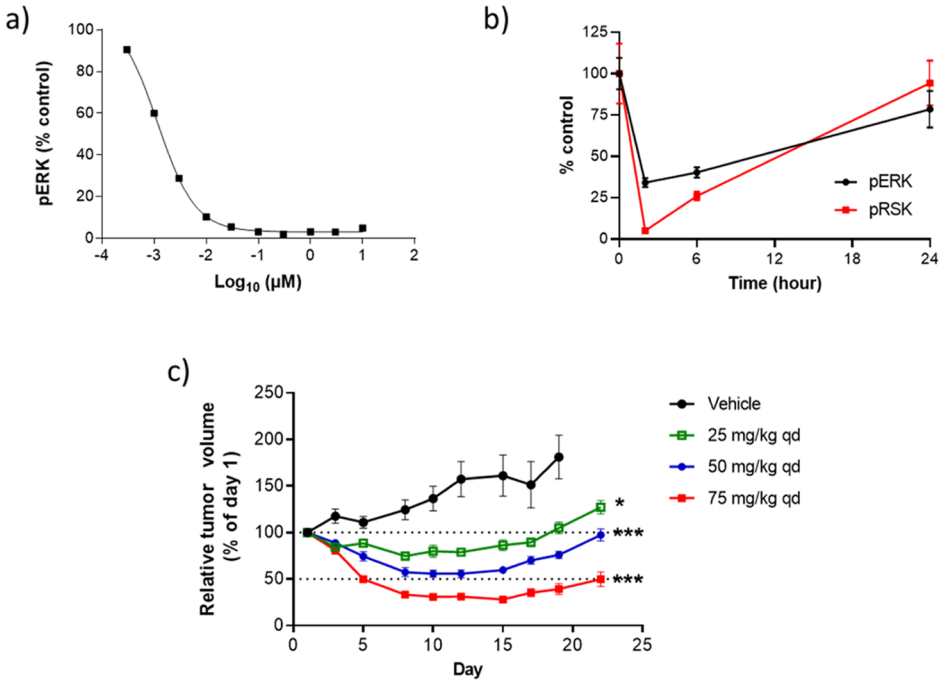

Figure 6. Compound **15** modulates pharmacodynamic markers of MAPK signaling and confers antitumor activity in a Colo205 subcutaneous xenograft model. (a) Levels of pERK in Colo205 cells after 2 h treatment with the indicated concentrations of compound **15**. (b) Mean tumor levels of pERK and pRSK after single oral dose of compound **15** administered at 50 mg/kg to mice bearing Colo205 xenografts. Each data point represents mean ± SD from three animals. (c) Inhibition of tumor growth following once daily (qd) oral dosing of compound **15** to mice bearing Colo205 xenografts. Each data point represents mean ± SEM from eight animals. *p < 0.05 and ***p < 0.001.

Pharmacodynamics and Efficacy. Overall, a number of compounds showed improved CYP3A4 half-life compared to the advanced lead compound **7**, and many of the compounds had comparable or superior pharmacokinetics and *in vitro* antiproliferative data. These compounds were selected for progression into *in vivo* PD and efficacy studies. Levels of phosphorylation of the ERK substrate pRSK were measured using MSD, while levels of pERK were determined by ELISA. Figure 6a gives a representative concentration response curve for pERK in the Colo205 mutant BRAF cell line for compound **15**. In general, the IC$_{50}$s for both pRSK and pERK in cellular assays tracked closely with the GI$_{50}$ values, reaching low nM values for the most potent compounds, and for this reason were not routinely collected (Table S1). In the *in vivo* PD assays using the Colo205 xenograft, the 3-fluoro-5-methoxyphenyl compound **15** clearly outperformed the analogues **17** and **20** with methoxy pyridine and piperazine-pyridyl groups, respectively, while analogues containing oxan replacements, including oxetane **22** and methoxypyridine **25**, also gave weaker responses than **15** (Figures 6b, S1). Triazole **24** also gave a weaker response than **15** in the PD assay (Figures 6b, S1), probably because at the 50 mg/kg dose; compound levels

https://doi.org/10.1021/acs.jmedchem.1c00905
J. Med. Chem. 2021, 64, 12286−12303

Table 5. Cross Species *In Vivo* Pharmacokinetic Parameters for Compound 15

	i.v.			p.o.					
species	dose (mg/kg)	Cl (mL/min/kg)	V_{dss} (L/kg)	dose (mg/kg)	$T_{1/2}$ (h)	T_{max} (h)	C_{max} (ng/mL)	AUC (ng h/mL)	F (%)
rat	0.50	18	0.77	1	1.5	0.5	25.76	57.94	6.1
				50	2.8	2.0	2743	17,460	35
				100	2.5	2.0	15,740	117,800	>100
dog	0.25	0.56	0.071	0.5	1.1	1.0	3664	12,320	91

Scheme 1[a]

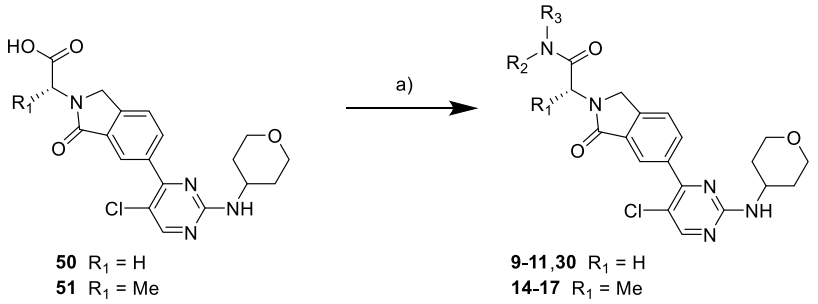

[a](a) From acid **50**: Compounds **9** (HATU, Et_3N, and DCM/DMF, chiral prep, 26%); **10** (44%); **11** (66%); and **30** (71%). From acid **51**: Compounds **14** (HATU, DIPEA, and DMF, 76%); **15** (TBTU, Et_3N, and DMF, 64%); **16** (TBTU, DIPEA, and DCM, 71%); and **17** (HATU, DIPEA, and DCM, 44%).

Scheme 2[a]

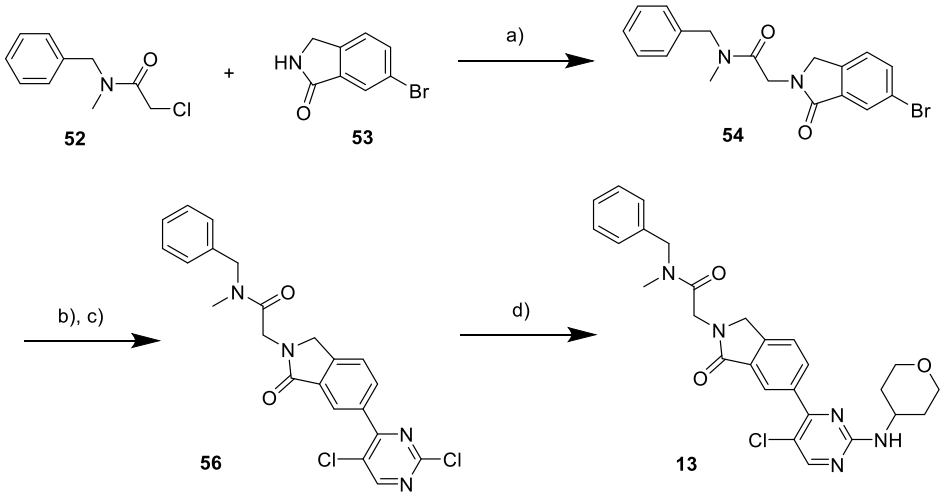

[a]a) NaH and DMF, ice bath. (b) $(Bpin)_2$, AcOK, $Pd(dppf)_2Cl_2$·DCM, and dioxane, 90 °C. (c) Trichloropyrimidine, K_2CO_3, dioxane/water, and $Pd(PPh_3)_4$, 100 °C. (d) 4-Aminooxan, DIPEA, and dioxane, 22% over four steps.

were not dose linear (data not shown) relative to the low dose PK shown in Table 4. We ascribed this to poor solubility leading to formulation challenges at the higher dose for compound **24**.

The performance in the PD assays translated into efficacy in the Colo205 xenograft tumor growth models. Compound **15** elicited tumor growth inhibition dose dependently in the range 25−75 mg/kg (Figure 6c).[22] Analogues **17**, **20**, and **25** also elicited tumor growth inhibition at their highest doses in the 75−100 mg/kg range and with a lesser overall effect than **15** (Figure S2). Compound **15** was therefore chosen as the most promising candidate due to its superior efficacy and PD response, together with its good pharmacokinetic parameters and robust *in vitro* data.

Further Characterization of ASTX029 (15). Given its promising performance in the Colo205 PD and efficacy models, compound **15** was selected for further characterization.[22] For example, compound **15** was shown to have good *in vivo* efficacy against six other xenografted cell lines. Additionally, compound **15** demonstrated high selectivity with only five kinases (excluding ERK1 and ERK2) which were inhibited to greater than 50% at 100 nM, when screened across a panel of 460 kinases.[22]

Broader selectivity was assessed using a Panlabs safety screen panel of 44 targets, all of which showed <50% inhibition at 10 μM, confirming the high selectivity of compound **15** (data not shown). Suspecting that highly active compounds in this series were too potent for accurate IC_{50} quantitation in the biochemical assay, we determined the binding constant using ITC titration, giving a K_d value of 0.47 nM (Figure S3).

Compound **15** demonstrated favorable pharmacokinetics in preclinical species (Table 5). In rat, compound **15**

https://doi.org/10.1021/acs.jmedchem.1c00905
J. Med. Chem. 2021, 64, 12286−12303

Scheme 3[a]

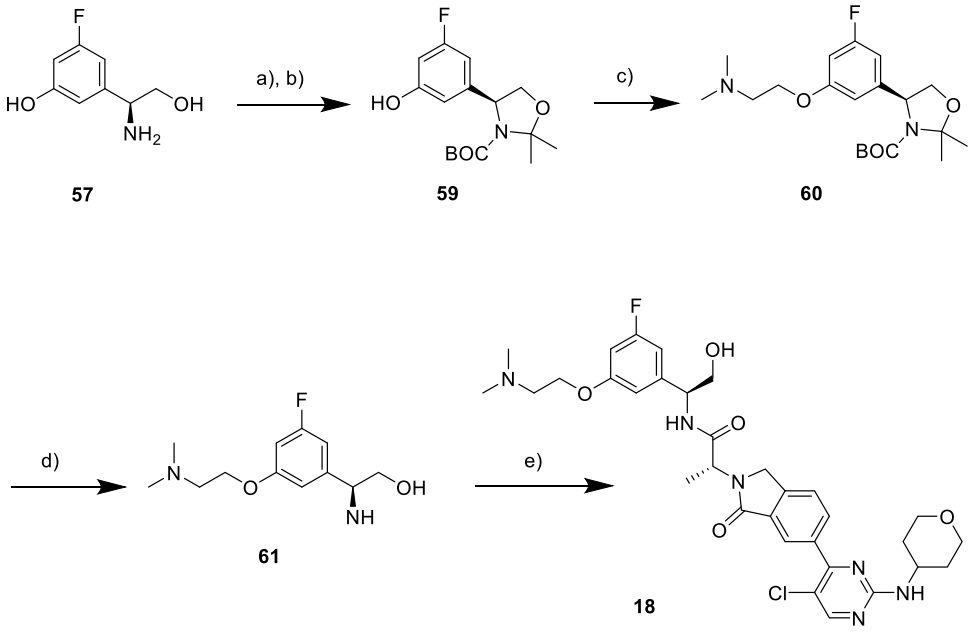

[a](a) BOC_2O, DCM, and DIPEA, 31%. (b) 2,2-Dimethoxypropane, TsOH, and DCM, 84%. (c) $Me_2N(CH_2)_2OMs$, NaH, and DMF, ice bath to room temp, 74%. (d) TFA and DCM, quant. (e) **51**, HATU, DIPEA, and DMF, 10%.

Scheme 4[a]

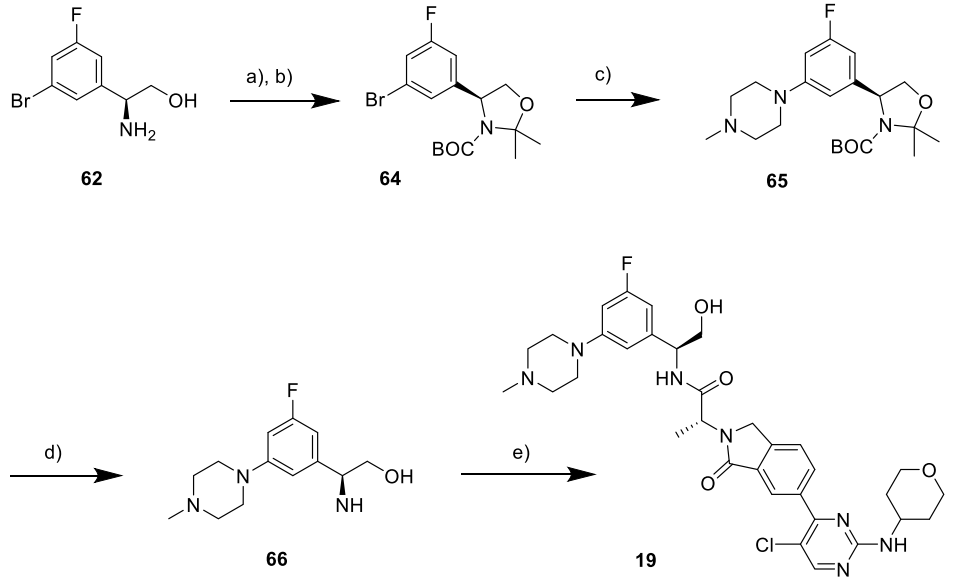

[a](a) BOC_2O, DCM, and DIPEA, 92%. (b) 2,2-Dimethoxypropane, TsOH, and DCM, 93%. (c) *N*-Methylpiperazine, Cs_2CO_3, Xantphos, and toluene, 120 °C, 14%. (d) HCl and EtOAc, quant. (e) **51**, TBTU, DIPEA, and DCM, 22%.

demonstrated supraproportional pharmacokinetics, possibly due to a reduction in the gastrointestinal and/or hepatic extraction ratio. *In vitro* to *in vivo* extrapolation (IVIVE) of hepatic clearance from intrinsic clearance measurements measured in microsomes and hepatocytes showed reasonable concordance with measured *in vivo* total clearance (data not shown). Human clearance was predicted to be low (<25% liver blood flow) based on IVIVE, and the predicted human dose based on exposures from mouse xenograft studies at 25 mg/kg was estimated to be approximately 500 mg.

Synthesis. Procedures for the preparation of compounds **7**, **8**, and **12** were described previously.[21] Compounds **9**−**11** and **30** were prepared by coupling the corresponding commercially available amines with the acid intermediate **50** (compound **42** in Heightman et al.[21]) (Scheme 1). Compounds **14**−**17** were prepared similarly from the respective commercial amines and the acid intermediate **51** (compound **48** in Heightman et al.[21]) (Scheme 1).

Compound **13** was prepared by an alternative, more convergent route (Scheme 2). Alkylation of 6-bromoisoquinolinone (**53**) with *N*-benzyl-2-chloro-*N*-benzylacetamide (**52**) to give **54** was followed by palladium-catalyzed borylation and Suzuki coupling to generate the dichloropyrimidine

https://doi.org/10.1021/acs.jmedchem.1c00905
J. Med. Chem. 2021, 64, 12286−12303

Scheme 5[a]

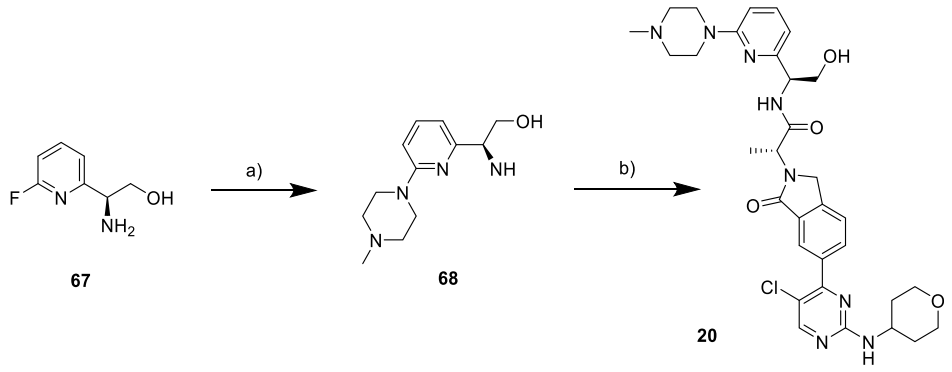

[a](a) *N*-Methylpiperazine and water, microwave 120 °C. (b) **51**, TBTU, DIPEA, and DCM, 61%.

Scheme 6[a]

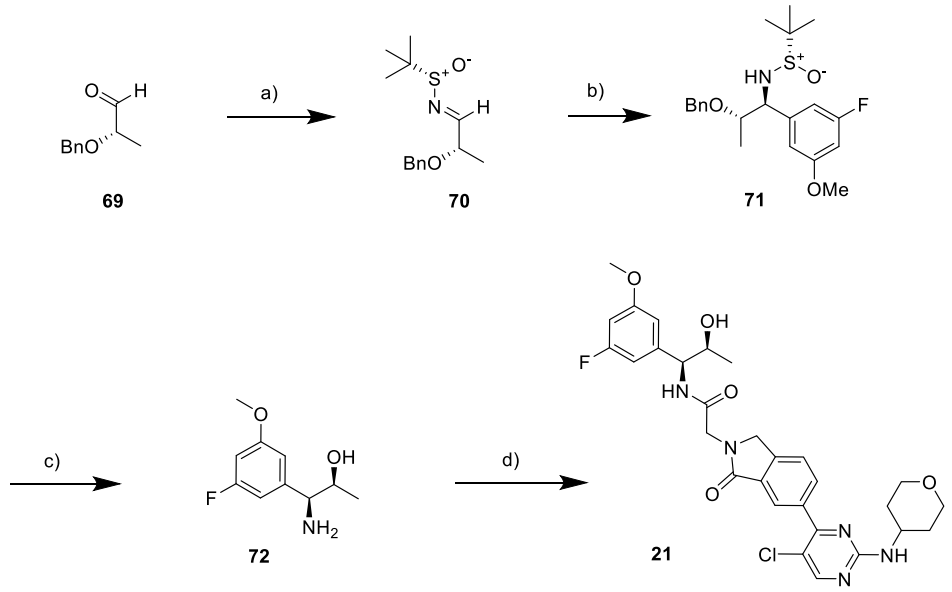

[a](a) (*S*)-^{t}Butyl sulfinamide, Ti(O^iPr)$_4$, and THF, 48%. (b) Stage 1: 1-Bromo-3-fluoro-5-methoxybenzene, Mg, and Et_2O, 30 °C; stage 2, −78 °C, addition to **70**, 61%. (c) HCl and MeOH and then HCl, MeOH, H_2 5 bar, and Pd/C, 58%. (d) **50**, TBTU, DIPEA, and DCM, 93%.

intermediate **56**. This allowed nucleophilic aromatic substitution with 4-amino-oxan to give **13**.

Compounds **18**−**20** required bespoke synthesis of the corresponding amines prior to coupling with acid **51**. The dimethylaminoethoxy compound **18** was prepared according to Scheme 3. BOC protection of commercial aminoalcohol **57** followed by acetonide formation gave the protected phenol **59** which was alkylated with 2-(dimethylamino)ethyl methanesulfonate to give the protected intermediate **60**. Acidic deprotection with TFA to give aminoalcohol **61** followed by HATU-mediated coupling with acid **51** afforded **18**. The phenylpiperazine **19** was synthesized according to Scheme 4. The bromofluorophenyl aminoalcohol **62** was subjected to a similar BOC and acetonide protection to give **64**, allowing Buchwald−Hartwig coupling with *N*-methylpiperazine to give **65**. Acidic deprotection with TFA and TBTU-mediated amide coupling gave **19**. Synthesis of the aminoalcohol intermediate **68** required for the pyridine analogue **20** did not require protection of the hydroxy and amino functions of the starting material **67**; instead, direct displacement of the fluoride was affected under microwave heating (Scheme 5). TBTU-mediated coupling of the product gave **20**.

The aminoalcohol for compound **21** was accessed using chiral sulfoximine chemistry (Scheme 6). Titanium(IV)-mediated condensation of (*S*)-2-methylpropane-2-sulfinamide (**69**) with (*S*)-2-(benzyloxy)propanal gave the distereomeric sulfinamide **70**, which was subject to addition by the Grignard reagent prepared from 1-bromo-3-ethoxy-5-fluorobenzene to give **71**. The desired aminoalcohol **72** was liberated by acidic desulfinylation followed by hydrogenolytic debenzylation. Finally, coupling with the acid **50** using TBTU gave **21** in good yield.

Compounds bearing alternative groups to oxan were assembled via alternative routes shown in Scheme 7. For the aliphatic analogues **22** and **26**, the chloropyrimidine acid intermediate **74** was first coupled with (*S*)-2-amino-2-(3-fluoro-5-methoxyphenyl)ethan-1-ol using TBTU to give the amide **75**, which was then subjected to S_NAR reaction with the appropriate amine. For the methylpyrazole analogue **23**, the aromatic amine was introduced by ^{t}Bu-BrettPhos-catalyzed Buchwald−Hartwig coupling, followed by acidic deprotection

https://doi.org/10.1021/acs.jmedchem.1c00905
J. Med. Chem. 2021, 64, 12286−12303

Scheme 7[a]

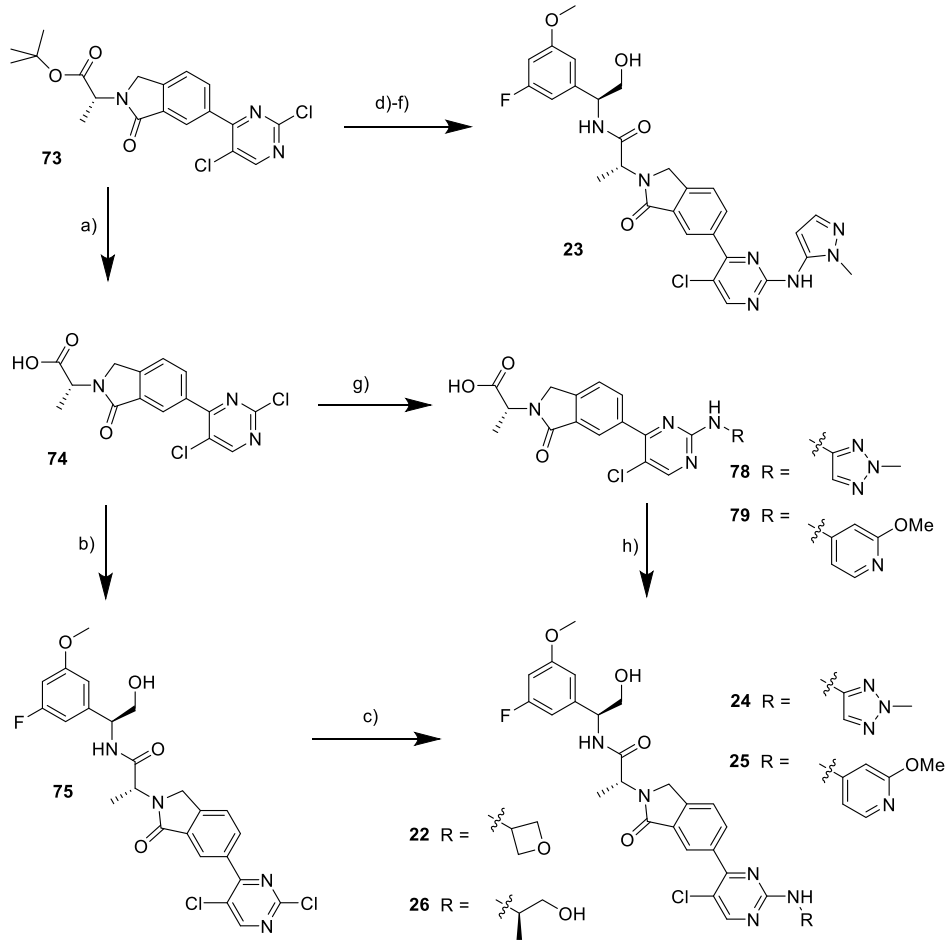

[a](a) TFA and DCM, 95%. (b) Amine, TBTU, DIPEA, and DCM, 80%. (c) **22**: oxetan-3-amine and EtOH, 80 °C, 90%; **26**: L-alaninol and EtOH, 80 °C, 15%. (d) 1-Methyl-1*H*-pyrazol-5-amine, Cs_2CO_3, *t*-BuBrettPhos allyl (Pd-175), and dioxane, 50 °C, 80%. (e) TFA and DCM, 88%. (f) Amine, TBTU, Et_3N, and DMF, 53%. (g) **78**: 2-methyl-2*H*-1,2,3-triazol-4-amine, Cs_2CO_3, *t*-BuBrettPhos allyl (Pd-175), and DMF, 70 °C, 72%; **79**: 2-methoxypyridin-4-amine, Cs_2CO_3, Xantphos, and DMF, 75 °C, 79%. (h) Amine, TBTU, DIPEA, and DMF; **24**: 79%; **25**: 82%.

Scheme 8[a]

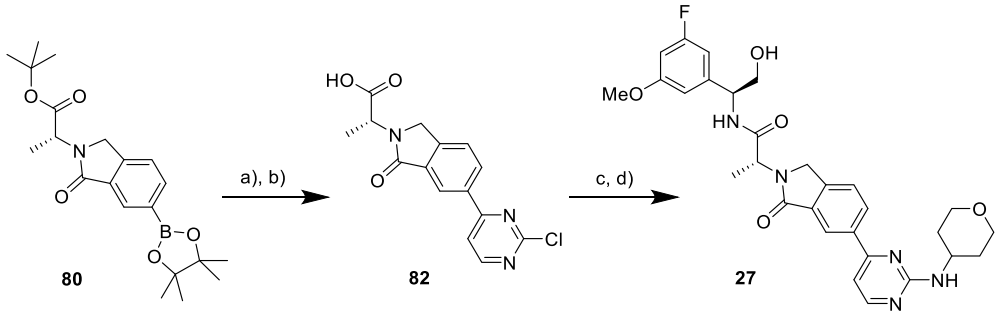

[a](a) 2,4-Dichloropyrimidine, Na_2CO_3, $Pd(PPh_3)_4$, and dioxane, 90 °C, 90%. (b) TFA and DCM, 98%. (c) Amine, TBTU, 4-methylmorpholine, and DMF, 41%. (d) Oxan-4-amine and DIPEA, 90 °C, 37%.

of the acid and final amide coupling. The methyl triazole and methoxypyridine analogues **24** and **25** were prepared similarly, except that the Buchwald−Hartwig couplings were carried out on the deprotected acid to avoid epimerization occurring alpha to the ester group.

The des-chloro analogue **27** was prepared according to Scheme 8. Suzuki coupling of the previously published boronate **80** with 2,4-dichloropyrimidine followed by acidic deprotection gave the acid intermediate **82**; then, amide coupling using TBTU followed by S_NAR reaction with oxan-4-amine provided **27**.

The aza-analogue **28** required a bespoke bicycle synthesis (Scheme 9). Starting from the bromochloropyridine **84**, a vinyl group was inserted using Molander chemistry and ozonolyzed to give the aldehyde **86**. Reductive amination with the *tert*-butyl ester of D-alanine gave the pyrrolopyridine intermediate

https://doi.org/10.1021/acs.jmedchem.1c00905
J. Med. Chem. 2021, 64, 12286−12303

Scheme 9[a]

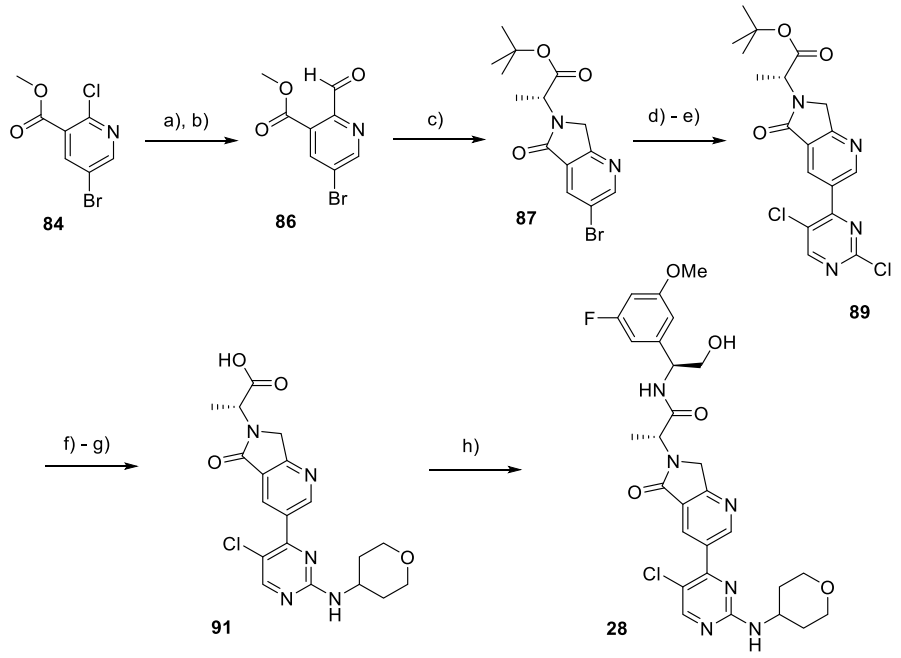

[a](a) $H_2C{=}CHBF_4K$, Et_3N, $PdCl_2(dppf)_2$, and EtOH, 90 °C, 51%. (b) Ozone and DCM, −78 °C, then Me_2S, warm to room temp, 64%. (c) (*R*)-*tert*-Butyl 2-aminopropanoate, DIPEA, and $NaB(OAc)_3H$, 40%. (d) $(Bpin)_2$, AcOK, $Pd(dppf)_2Cl_2$·DCM, and dioxane, 90 °C, 82%. (e) Trichloropyrimidine, Na_2CO_3, $Pd(PPh_3)_4$, and dioxane, 90 °C. (f) Oxan-4-amine, DIPEA, and dioxane, 90 °C, 66% over two steps. (g) TFA and DCM, 94%. (h) Amine, TBTU, DIPEA, and DMF, 33%.

Scheme 10[a]

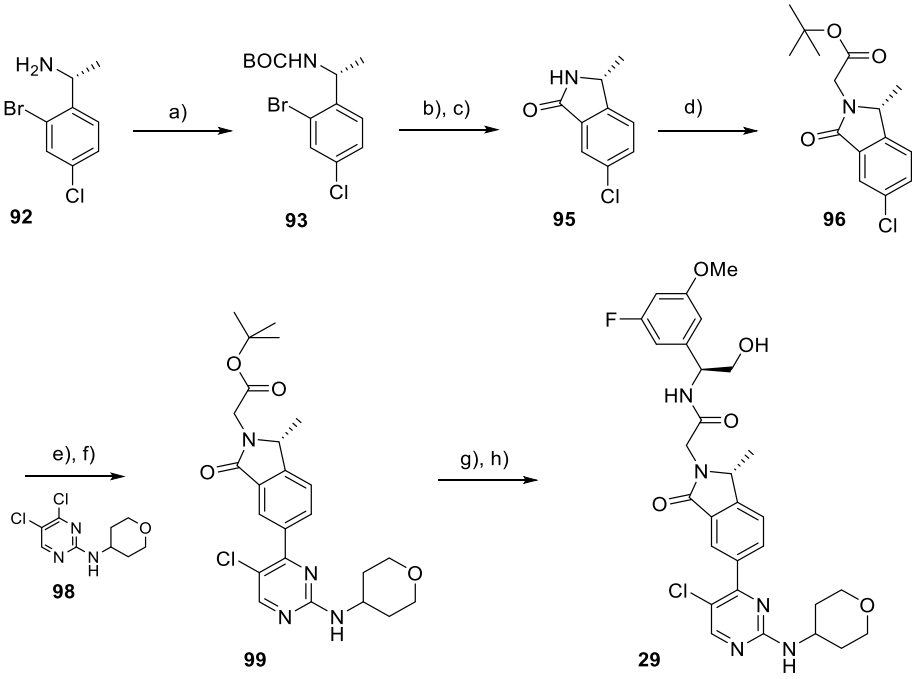

[a](a) BOC_2O, DCM, and DIPEA, 95%. (b) CO, $([Ph_2P]_2CH_2CH_2)_2$, $Pd(OAc)_2$, and DMF, 90 °C. (c) TFA and DCM, 56% over two steps. (d) $BrCH_2CO_2{}^tBu$, NaH, and DMF, ice bath warms to room temp, 63%. (e) $(Bpin)_2$, AcOK, Pd(crotyl) (XPhos)Cl, and dioxane, 90 °C. (f) **98**, Na_2CO_3, $Pd(PPh_3)_4$, and dioxane, 90 °C, 49% over two steps. (g) TFA and DCM, quant. (h) Amine, TBTU, Et_3N, and DCM, 64%.

87. Palladium-catalyzed borylation allowed Suzuki−Miyaura coupling to generate the dichloropyridine **89**, which was subjected to S_NAR with oxan-4-amine and acidic deprotection to afford acid **91**. Finally, amide coupling with TBTU as before gave **28**.

The 3-methyl-substituted isoindolinone **29** also required bespoke synthesis of the core (Scheme 10). The (*R*)-bromo-chloro *α*-methylbenzylamine **92** was BOC-protected, and then, palladium-catalyzed carbonylation and deprotection gave the chiral 6-chloro-3-methylisoindolinone **95**. Alkylation with *tert*-

https://doi.org/10.1021/acs.jmedchem.1c00905
J. Med. Chem. 2021, 64, 12286−12303

butyl bromoacetate gave intermediate **96**, which was borylated as before and then coupled with the oxanyl dichloropyrimidine **98** to give ester **99**. Acidic deprotection and amide coupling with TBTU as before gave **29**.

CONCLUSIONS

Our optimization strategy was driven by knowledge of metabolic weaknesses in the lead molecule **7** together with multiparameter optimization based on empirical data collected across analogues within the lead series. Structure-based drug design was also employed to narrow down the number of plausible options in the lead optimization campaign, and crystal structures in complex with ERK2 identified potential sites for chemical modification to modulate the metabolic profile, while maintaining potency. The metabolism studies highlighted the oxan ring as a key site of metabolism in lead molecule **7**; however, replacement with more metabolically stable isosteres produced compounds with inferior solubility, consistent with previous observations on the need to maintain sufficient sp^3 character in drug molecules.[25,26] Finally, retaining the oxan group while replacing the tolyl group, the other key site of metabolic instability, with the 3-fluoro-5-methoxyphenyl group in **15** provided sufficient metabolic stabilization in *in vitro* models while maintaining favorable potency and physicochemical properties. Although the oxan ring has been associated with metabolic instability due to a propensity for oxidative metabolism in alpha position to the ring oxygen atom,[27] this issue appears to be context-dependent, and there are now a significant number of drugs incorporating this group that show good pharmacokinetics with long half-lives in humans, including venetoclax[28] and gilteritinib.[29]

A combination of cellular antiproliferative potency data and total plasma exposure was sufficient to predict compounds showing the strongest pharmacodynamic response, which correlated with efficacy in tumor xenografts. Compound **15** possessed the most favorable balance of performance in efficacy models of both BRAF and KRas mutant cancers with the selectivity and preclinical pharmacokinetic profile, leading to its selection as a clinical candidate. Compound **15** is currently in a phase I–II clinical trial in patients with advanced solid malignancies who are not candidates for approved or available therapies.[30]

EXPERIMENTAL PROCEDURES

Protein Expression, Purification, and Crystallography. Full-length human ERK2 (hERK2) was cloned into pET30a with a noncleavable MAHHHHHH N-terminal tag. hERK2 was expressed in *Escherichia coli* BL21(DE3), and nonphosphorylated hERK2 (confirmed by) was purified using sequential Ni-HiTRAP, desalt, Resource-Q, and S75 26/60 column steps. hERK2 was crystallized under conditions adapted from Aronov et al.,[31] and crystals were soaked in a solution equivalent to the crystallization solution but also containing 0.1–100 mM ligand, 10 mM DTT, and 10% DMSO final. Crystals were cryo-protected using crystallization solution containing 35% 2KMPEG final. X-ray diffraction data were collected using both in-house and synchrotron X-ray sources.

ERK2 Kinase Assay. ERK2 kinase activity was determined using a TRF activity assay. The ERK2 enzyme (0.25 nM) was incubated with the substrates ATF2-GFP (0.4 μM) and ATP (20 μM) in 50 mM Tris pH7.5, 10 mM $MgCl_2$, 1 mM EGTA, 0.01% Triton X100, 1 mM DTT, and 2.5% DMSO, with shaking at room temperature for 30 min. Reactions were stopped by the addition of a stop and detection mix, containing 25 mM EDTA and 2 nM Tb-pATF2 antibody in TR-FRET dilution buffer (Life Technologies, Paisley, UK), and the plate was incubated with shaking at room temperature for 1 h. Upon excitation at 340 nm, fluorescence was measured at 520 nm (A counts) and 495 nm (B counts) using a Pherastar plate reader (BMG Labtech, Ortenberg, Germany).

Cell Culture and Reagents. The human cell lines A375 and Colo205 were purchased from the American Type Culture Collection (ATCC, Manassas, VA, USA) and the European Collection of Authenticated Cell Cultures (ECACC Salisbury, UK), respectively. The cells lines were not passaged for more than 6 months after authentication by the cell banks (DNA fingerprinting and cytogenetic analysis or short-tandem repeat PCR). Both cell lines were grown in DMEM culture medium, supplemented with 10% FBS (Thermo Fisher Scientific, Waltham, Massachusetts, USA) and maintained at 37 °C in an atmosphere of 5% CO_2.

Cell Proliferation Assay. Cell proliferation assays were carried out using Alamar Blue (Thermo Fisher Scientific, Waltham, Massachusetts, USA) as described previously.[32] Briefly, 5×10^3 cells were seeded in complete culture medium into flat-bottomed 96-well plates, 1 day before the drug treatment. Cells were incubated with the compound in 0.1% (v/v) dimethyl sulfoxide (DMSO) for 96 h before viability was assessed using Alamar blue. IC_{50} values were calculated using a sigmoidal dose response equation (Prism GraphPad software, La Jolla, CA, USA).

***In Vitro* Permeability.** Permeability of test compounds was assessed using the CacoReady system. Test and control compounds (propranolol, antipyrine, and vinblastine) were incubated at a final concentration of 10 μM in duplicate to either the apical (180 μL) of the monolayer to measure apical to basolateral transport (A > B) across the cell barrier or to the basolateral side (750 μL) to measure the basolateral to apical transport (B > A). For A > B spiking, test and control compounds were diluted from 10 mM DMSO stocks to 10 μM in Hanks' balanced salt solution buffer with 100 mM $CaCl_2 \cdot 2H_2O$, 50 mM $MgCl_2 \cdot 5H_2O$, and 0.5 mg/mL Lucifer yellow made to volume with sterile water (Lucifer yellow was used to determine the integrity of the Caco-2 monolayer). For B > A compound spiking, test and control compounds were prepared as for the A > B solutions without the addition of Lucifer yellow. Test and control compounds were incubated for 1 h at 37 °C in a highly humidified atmosphere of 95% air and 5% CO_2.

Quantification of pRSK by MSD. A375 cells were seeded at 1.5×10^4 cells per well into 96-well plates and allowed to recover for 16 h, prior to the addition of compounds (in 0.1% DMSO v/v) and incubation for a further 4 h. Cells were lysed by adding cell lysis buffer (Cell Signaling Technology, Massachusetts, USA) and incubating at room temperature for 20 min. Custom MSD plates (Meso Scale Discovery, Maryland, USA) precoated with the anti-pRSK antibody (Cell Signaling Technology, Massachusetts, USA) were blocked with kit blocking buffer for 1 h at room temperature, prior to washing. Equivalent amounts of protein lysate were added to the blocked plates and incubated for 3 h at room temperature. After washing, plates were incubated for 1 h at room temperature with sulfo-tag-conjugated anti-RSK detection antibodies (R&D Systems, Minneapolis, USA). Plates were washed, and read buffer was added before reading the plate on a MESO QuickPlex SQ 120 (Meso Scale Discovery, Maryland, USA). IC_{50} values were calculated using a sigmoidal dose response equation (Prism GraphPad software, La Jolla, CA, USA). For pharmacodynamic studies, Colo205 xenograft tumor lysates were prepared as described above and transferred directly to Custom MSD pRSK plates (Meso Scale Discovery, Maryland, USA) for analysis.

Quantification of pERK by ELISA. A375 cells were treated with compounds and lysed as described above. Lysates were then cleared by centrifugation, transferred to pERK ELISA plates (Cell Signaling Technology, Massachusetts, USA), and analyzed according to the manufacturer's instructions. IC_{50} values were calculated using a sigmoidal dose response equation (Prism GraphPad software, La Jolla, CA, USA). For pharmacodynamic studies, Colo205 xenograft tumor lysates were prepared as described above, transferred to pERK ELISA plates (Cell Signaling Technology, Massachusetts, USA), and analyzed according to the manufacturer's instructions.

***In Vivo* Studies.** The care and treatment of experimental animals were in accordance with the United Kingdom Coordinating

https://doi.org/10.1021/acs.jmedchem.1c00905
J. Med. Chem. 2021, 64, 12286–12303

Committee for Cancer Research guidelines[33] and the United Kingdom Animals (Scientific Procedures) Act 1986.[34] Animals had access to food and water ad libitum throughout the acclimatization and study period.

Pharmacokinetic Studies. Pharmacokinetic studies were performed in male BALB/c mice, obtained from Harlan Laboratories Inc. (Shardlow, UK). Pharmacokinetic studies in male rats (Sprague−Dawley and Hans Wistar) and male Beagle dogs were performed by either Quotient Bioresearch (Rushden, UK) or Aptuit (Verona, Italy). For intravenous administrations in mice, test compounds were formulated in either 20% DMA/80% saline, 10% DMSO/20% PEG400/70% water, or 10% DMSO/90% saline. For oral administrations in mice, test compounds were formulated in either 10% ethanol/10% cremaphor/10% PEG200/70% water, 20% PEG400/80% HPMC, or 10% DMSO/20% cremaphor/70% saline. Intravenous dosing at 0.5 mg/kg was administered via the lateral tail vein at a dose volume of 5 mL/kg. Test compounds were administered orally at 5 mg/kg by nasogastric gavage at a dose volume of 10 mL/kg. Compound **15** was administered to rats either intravenously at 0.5 mg/kg (n = 3) or via oral gavage at 1, 50, and 100 mg/kg (n = 3), at a dose volume of 5 mL/kg, formulated in 10% DMSO and 90% saline or 10% NMP, 15% PEG200 and 75% methylcellulose (1% aq, w/v), and 75% PEG 400 and 25% water or 100% PEG400, respectively. In male Beagle dogs, compound **15** was administered intravenously at 0.25 mg/kg or via oral gavage at 0.5 mg/kg, at a dose volume of 5 mL/kg, formulated in 10% NMP, 20% PEG200 and 70% saline or 10% NMP, 15% PEG200 and 75% water, respectively. A week wash-out period was included between dosing (n = 3). All doses were calculated as freebase equivalent per kg of bodyweight. Following dosing, blood samples were drawn into tubes containing potassium EDTA via either saphenous vein bleeding or cardiac puncture at various time points over 24 h using sparse sampling (n = 3 per time point) in mice, via tail vein and cardiac puncture in rats, or via jugular vein in dogs using serial sampling. Blood samples were centrifuged (2000g at 4 °C, 10 min), and the resultant plasma was separated from the erythrocyte pellets for analysis and stored at −20 °C. Noncompartmental pharmacokinetic (PK) analyses were performed using Phoenix 6.3.0.395 (Certara USA, Inc.) software.

***In Vitro* Phenotyping.** Test compounds were incubated (1 μM) in human Supersomes expressing (0.25 mg/mL) CYP isozymes (20 pmol/mL; CYP3A4, CYP2D6, CYP2C9, CYP2C8, CYP1A2, CYP2B6, and CYP2C19) in the presence of NADPH at +37 °C for 40 min. Samples were taken at 0, 5, 10, 20, and 40 min, and protein was precipitated with acetonitrile and centrifuged prior to bioanalysis.

***In Vitro* Microsomal Stability.** The test compound and the positive control, diclofenac, were incubated in duplicate at 1 μM in male CD-1 mouse and mixed gender human liver microsomes at 37 °C for 40 min at a microsomal protein concentration of 0.25 mg/mL, in the presence of NADPH and UDPGA. In addition, compound **15** was incubated in male Sprague−Dawley rat and male Beagle dog liver microsomes under the same conditions. Negative control incubations, in the absence of NADPH and UDPGA, were performed. Incubations were sampled (50 μL) at 0, 5, 10, 20, and 40 min, except for the negative controls which were sampled at 0 and 40 min.

***In Vitro* Hepatocyte Stability.** Compound **15** and the positive controls, verapamil and umbelliferone, were incubated in duplicate at 1 μM in male CD-1 mouse, male Sprague−Dawley rat, and male Beagle dog and at 0.2, 1, and 10 μM in mixed gender human cryopreserved hepatocytes at 37 °C for 60 min. Williams E media supplemented with 2 mM L-glutamine and 25 mM HEPES and test compounds (final DMSO concentration, 0.25%) were preincubated at 37 °C prior to the addition of a suspension of cryopreserved hepatocytes (final cell density of 0.5×10^6 viable cells/mL in Williams E media supplemented with 2 mM L-glutamine and 25 mM HEPES) to initiate the reaction. The final incubation volume was 500 μL. Aliquots (50 μL) were sampled at timed intervals (0, 5, 10, 20, 40, and 60 min) from each incubation. Negative vehicle controls were included.

Xenograft Studies. Colo205 xenografts were prepared by subcutaneously injecting 5×10^6 cells suspended in serum-free medium mixed 1:1 with Matrigel (BD Biosciences, San Jose, CA, USA) into the right flank of each male BALB/c nude mouse. Tumors were measured using caliper and tumor volumes calculated by applying the formula for an ellipsoid. For efficacy studies, when the tumors reached an average of approximately 200 mm^3, mice were randomized into groups of eight. Mice were dosed orally once a day at a dose of 25−75 mg/kg compound **15**, 100 mg/kg compound **17** and **25**, and 75 mg/kg compound **20**. Body weights were recorded daily, and tumor volumes were measured every 3−4 days. For PK/PD studies, a single dose of compound was administered orally to mice. For oral administrations in PD or efficacy studies, test compounds were formulated in either 20% PEG200/0.5% Methocel or 75% PEG200/25% water or 10% NMP/15% PEG200/0.75% Methocel. Following dosing, blood samples were drawn in tubes containing potassium EDTA via either saphenous vein bleeding or cardiac puncture at various time points, prior to centrifugation (2000g at 4 °C, 10 min). The resultant plasma was separated from the erythrocyte pellets for analysis and stored at −20 °C. Tumors were immediately excised and flash-frozen in liquid nitrogen.

Bioanalysis. All *in vitro* and *in vivo* samples were extracted by protein precipitation with the acetonitrile-containing internal standard (1:3 v/v). For quantitative studies, calibration standards and quality controls were prepared in the blank matrix and extracted under the same conditions. All samples were centrifuged at 3700 rpm at 4 °C for 20 min. Compound bioanalysis of all *in vitro* and *in vivo* samples was performed using high-performance liquid chromatography mass spectrometry (LC/MS). Test compounds and the internal standard were ionized using positive-mode (ESI^+) electrospray ionization. Analytes were detected using multiple reaction monitoring. Test compounds typically ran on a gradient HPLC method over 5 min with 10 mM ammonium acetate and acetonitrile mobile phase at a flow rate of 0.5 mL/min. Separation was typically achieved using an Acquity HSS T3 1.8 μM 50 × 2.1 mm column maintained at 40 °C.

Prediction of Human Pharmacokinetics. Microsomal and hepatocyte intrinsic clearance in preclinical species was scaled to total hepatic clearance using the well-stirred model[35] to generate a prediction of human clearance. Human dose was predicted using the target AUC and was taken from efficacy studies in mouse xenograft models, using the average bioavailability determined in preclinical studies.

Synthesis. *General Procedures.* All solvents and commercially available reagents were used as received. All reactions were followed by thin-layer chromatography (TLC) analysis (TLC plates GF254, Merck) or LC−MS (liquid chromatography mass spectrometry). LC−MS analysis was performed with an Agilent or Shimadzu LC system with variable wavelength UV detection using reverse-phase chromatography with a CH_3CN and water gradient with a 0.02 or 0.1% TFA modifier (added to each solvent) and using a reverse-phase column, for example, Thermo Hypersil Gold C18. MS was determined using either PE Sciex 150EX LC−MS, Waters ZQ LC−MS, or Agilent 6140 LC−MS Single Quadrupole instruments. Column chromatography was performed on prepacked silica gel columns (3090 mesh, IST) using a Biotage SP4 or similar. NMR spectra are referenced as follows: ^1H (400 MHz), internal standard TMS at δ = 0.00. Abbreviations for multiplicities observed in NMR spectra are as follows: s; singlet; br s, broad singlet; d, doublet; t, triplet; q, quadruplet; p, pentuplet; and m, multiplet. All compounds reported are of at least 95% purity according to LC−MS unless stated otherwise.

*(2R)-2-(6-(5-Chloro-2-[(oxan-4-yl)amino]pyrimidin-4-yl)-1-oxo-2,3-dihydro-1H-isoindol-2-yl)-N-[(1S)-1-(3-fluoro-5-methoxyphenyl)-2-hydroxyethyl]propanamide (**15**).* A stirred solution of (*R*)-2-(6-(5-chloro-2-((oxan-**4**-yl)amino)pyrimidin-4-yl)-1-oxoisoindolin-2-yl)propanoic acid (compound **48** in Heightman et al.[21]) (70 mg, 0.168 mmol), (*S*)-2-amino-2-(3-fluoro-5-methoxyphenyl)ethanol·HCl (41 mg, 0.185 mmol), and triethylamine (0.094 mL, 0.672 mmol) in DMF (1 mL) was treated with TBTU (65 mg, 0.202 mmol) and stirred at room temperature overnight. The mixture was diluted

https://doi.org/10.1021/acs.jmedchem.1c00905
J. Med. Chem. 2021, 64, 12286−12303

with ethyl acetate (20 mL), was washed successively with 1 M $KHSO_4$ (10 mL), $NaHCO_3$ (10 mL), brine (2 × 10 mL), and then water (4 × 10 mL), was dried ($MgSO_4$), and evaporated. The residue was purified by chromatography (SiO_2, 12 g column, 0–5% EtOH in EtOAc) to give a glass, which was triturated with ether (2 mL) to give a solid. The solid was collected by filtration, washed with ether (2 × 1 mL), and dried under vacuum at 50 °C overnight to give the title compound (64.3 mg, 64.3%) as a cream solid. ^{1}H NMR (DMSO-d_6): δ 8.54 (d, J = 8.1 Hz, 1H), 8.44 (s, 1H), 8.04 (d, J = 1.6 Hz, 1H), 7.97 (dd, J = 7.9, 1.7 Hz, 1H), 7.74 (d, J = 7.9 Hz, 1H), 7.59 (d, J = 5.6 Hz, 1H), 6.76–6.66 (m, 3H), 4.99 (q, J = 7.2 Hz, 1H), 4.90 (t, J = 5.5 Hz, 1H), 4.81 (q, J = 6.6 Hz, 1H), 4.75 (d, J = 18.1 Hz, 1H), 4.61 (d, J = 18.1 Hz, 1H), 3.99–3.88 (m, 1H), 3.86 (dt, J = 11.3, 3.4 Hz, 2H), 3.76 (s, 3H), 3.61–3.49 (m, 2H), 3.44–3.33 (m, 2H), 1.91–1.78 (m, 2H), 1.60–1.47 (m, 2H), 1.45 (d, J = 7.2 Hz, 3H). ^{13}C NMR (101 MHz, DMSO-d_6): δ 170.8, 166.9, 162.8 (d, J = 242.0 Hz), 161.4 (very broad), 160.4 (d, J = 11.6 Hz), 160.0, 158.2 (very broad), 144.6 (d, J = 8.9 Hz), 143.9, 135.9 (very broad), 132.0, 132.0, 123.4, 123.1, 114.7, 109.0 (d, J = 2.4 Hz), 105.6 (d, J = 22.2 Hz), 99.8 (d, J = 25.2 Hz), 66.0, 64.3, 55.5, 54.8 (d, J = 2.2 Hz), 49.6, 47.2, 47.1, 32.3, 16.2. LCMS: $[M + H]^+$ 584. HRMS (ESI-QTOF): m/z $[M + H]^+$ calcd for $C_{29}H_{31}ClFN_5O_5$ 584.2069; found, 584.2065. Δ = −0.75 ppm.

■ ASSOCIATED CONTENT

Supporting Information

The Supporting Information is available free of charge at https://pubs.acs.org/doi/10.1021/acs.jmedchem.1c00905.

Cellular pRSK and pERK IC_{50} values for selected compounds; PK/PD data for compounds **17**, **20**, **22**, **24**, and **25**; antitumor efficacy data for compounds **17**, **20**, and **25**; ITC titration of compound **15**; HPLC trace for compound **15**; information on reproducibility for the ERK2 enzyme and A375 cell assays; and synthesis of compounds **9**–**11**, **13**, **14**, **16**–**30**, and associated intermediates (PDF)

Molecular formula strings (CSV)

■ AUTHOR INFORMATION

Corresponding Author

Christopher W. Murray − *Astex Pharmaceuticals, Cambridge CB4 0QA, U.K.*; orcid.org/0000-0003-3733-0700; Phone: +44 (0) 1223 226228; Email: Chris.Murray@astx.com; Fax: +44 (0) 1223 226201

Authors

Tom D. Heightman − *Astex Pharmaceuticals, Cambridge CB4 0QA, U.K.*

Valerio Berdini − *Astex Pharmaceuticals, Cambridge CB4 0QA, U.K.*

Luke Bevan − *Astex Pharmaceuticals, Cambridge CB4 0QA, U.K.*

Ildiko M. Buck − *Astex Pharmaceuticals, Cambridge CB4 0QA, U.K.*

Maria G. Carr − *Astex Pharmaceuticals, Cambridge CB4 0QA, U.K.*

Aurélie Courtin − *Astex Pharmaceuticals, Cambridge CB4 0QA, U.K.*

Joseph E. Coyle − *Astex Pharmaceuticals, Cambridge CB4 0QA, U.K.*

James E. H. Day − *Astex Pharmaceuticals, Cambridge CB4 0QA, U.K.*

Charlotte East − *Astex Pharmaceuticals, Cambridge CB4 0QA, U.K.*

Lynsey Fazal − *Astex Pharmaceuticals, Cambridge CB4 0QA, U.K.*

Charlotte M. Griffiths-Jones − *Astex Pharmaceuticals, Cambridge CB4 0QA, U.K.*

Steven Howard − *Astex Pharmaceuticals, Cambridge CB4 0QA, U.K.*

Justyna Kucia-Tran − *Astex Pharmaceuticals, Cambridge CB4 0QA, U.K.*

Vanessa Martins − *Astex Pharmaceuticals, Cambridge CB4 0QA, U.K.*

Sandra Muench − *Astex Pharmaceuticals, Cambridge CB4 0QA, U.K.*

Joanne M. Munck − *Astex Pharmaceuticals, Cambridge CB4 0QA, U.K.*

David Norton − *Astex Pharmaceuticals, Cambridge CB4 0QA, U.K.*; orcid.org/0000-0002-8680-4936

Marc O'Reilly − *Astex Pharmaceuticals, Cambridge CB4 0QA, U.K.*

Nicholas Palmer − *Astex Pharmaceuticals, Cambridge CB4 0QA, U.K.*

Puja Pathuri − *Astex Pharmaceuticals, Cambridge CB4 0QA, U.K.*

Torren M. Peakman − *Astex Pharmaceuticals, Cambridge CB4 0QA, U.K.*

Michael Reader − *Astex Pharmaceuticals, Cambridge CB4 0QA, U.K.*

David C. Rees − *Astex Pharmaceuticals, Cambridge CB4 0QA, U.K.*

Sharna J. Rich − *Astex Pharmaceuticals, Cambridge CB4 0QA, U.K.*

Alpesh Shah − *Astex Pharmaceuticals, Cambridge CB4 0QA, U.K.*

Nicola G. Wallis − *Astex Pharmaceuticals, Cambridge CB4 0QA, U.K.*

Hugh Walton − *Astex Pharmaceuticals, Cambridge CB4 0QA, U.K.*

Nicola E. Wilsher − *Astex Pharmaceuticals, Cambridge CB4 0QA, U.K.*

Alison J.-A. Woolford − *Astex Pharmaceuticals, Cambridge CB4 0QA, U.K.*; orcid.org/0000-0002-6453-5819

Michael Cooke − *Sygnature Discovery Ltd., Nottingham NG1 1GF, U.K.*

David Cousin − *Sygnature Discovery Ltd., Nottingham NG1 1GF, U.K.*

Stuart Onions − *Sygnature Discovery Ltd., Nottingham NG1 1GF, U.K.*

Jonathan Shannon − *Sygnature Discovery Ltd., Nottingham NG1 1GF, U.K.*

John Watts − *Sygnature Discovery Ltd., Nottingham NG1 1GF, U.K.*

Complete contact information is available at: https://pubs.acs.org/10.1021/acs.jmedchem.1c00905

Notes

The authors declare no competing financial interest.

Coordinates and structure factors for the ERK2-ligand complex have been deposited with PDB with the following accession codes: **9**, 7NQQ; **10**, 7NQW; **11**, 7NR3; **17**, 7NR9; **20**, 7NR8; and **24**, 7NR5. Authors will release the atomic coordinates and experimental data upon article publication.

■ ACKNOWLEDGMENTS

We would like to acknowledge Anne Cleasby for technical help in preparing the X-ray structures for deposition.

ABBREVIATIONS

BRAF, B-Raf proto-oncogene; DMSO, dimethyl sulfoxide; DSF, differential scanning fluorimetry; ERK, extracellular signal-related kinase; HATU, 1-[bis(dimethylamino)-methylene]-1*H*-1,2,3-triazolo[4,5-*b*]pyridinium 3-oxid hexafluorophosphate; HBSS, Hanks' balanced salt solution; HBTU, *N*,*N*,*N*′,*N*′-tetramethyl-*O*-(1*H*-benzotriazol-1-yl)-uronium hexafluorophosphate; HPMC, hydroxypropyl methylcellulose; IVIVE, *in vitro* to *in vivo* extrapolation; MAPK, mitogen-activated protein kinase; MEK, mitogen activated protein kinase; MSD, mesoscale discovery; RAS, retrovirus-associated DNA sequence; RSK, ribosomal S6 kinase; T3P, 2,4,6-tripropyl-1,3,5,2,4,6-trioxatriphosphorinane-2,4,6-trioxide; TBTU, 2-(1*H*-benzotriazole-1-yl)-1,1,3,3-tetramethyluronium tetrafluoroborate; TRF, time-resolved fluorescence

REFERENCES

(1) Samatar, A. A.; Poulikakos, P. I. Targeting ras−erk signalling in cancer: Promises and challenges. *Nat. Rev. Drug Discovery* **2014**, *13*, 928.

(2) Payne, D. M.; Rossomando, A. J.; Martino, P.; Erickson, A. K.; Her, J. H.; Shabanowitz, J.; Hunt, D. F.; Weber, M. J.; Sturgill, T. W. Identification of the regulatory phosphorylation sites in pp42/mitogen-activated protein kinase (map kinase). *EMBO J.* **1991**, *10*, 885−892.

(3) Eblen, S. T. Chapter four—Extracellular-regulated kinases: Signaling from ras to erk substrates to control biological outcomes. In *Advances in Cancer Research*; Tew, K. D., Fisher, P. B., Eds.; Academic Press, 2018; Vol. *138*, pp 99−142.

(4) Ryan, M. B.; Der, C. J.; Wang-Gillam, A.; Cox, A. D. Targeting ras-mutant cancers: Is erk the key? *Trends Cancer* **2015**, *1*, 183−198.

(5) Robert, C.; Grob, J. J.; Stroyakovskiy, D.; Karaszewska, B.; Hauschild, A.; Levchenko, E.; Chiarion Sileni, V.; Schachter, J.; Garbe, C.; Bondarenko, I.; Gogas, H.; Mandalá, M.; Haanen, J. B. A. G.; Lebbé, C.; Mackiewicz, A.; Rutkowski, P.; Nathan, P. D.; Ribas, A.; Davies, M. A.; Flaherty, K. T.; Burgess, P.; Tan, M.; Gasal, E.; Voi, M.; Schadendorf, D.; Long, G. V. Five-year outcomes with dabrafenib plus trametinib in metastatic melanoma. *N. Engl. J. Med.* **2019**, *381*, 626−636.

(6) Caunt, C. J.; Sale, M. J.; Smith, P. D.; Cook, S. J. Mek1 and mek2 inhibitors and cancer therapy: The long and winding road. *Nat. Rev. Cancer* **2015**, *15*, 577.

(7) Kidger, A. M.; Sipthorp, J.; Cook, S. J. Erk1/2 inhibitors: New weapons to inhibit the ras-regulated raf-mek1/2-erk1/2 pathway. *Pharmacol. Ther.* **2018**, *187*, 45−60.

(8) Roskoski, R. Targeting erk1/2 protein-serine/threonine kinases in human cancers. *Pharmacol. Res.* **2019**, *142*, 151−168.

(9) Sullivan, R. J.; Infante, J. R.; Janku, F.; Wong, D. J. L.; Sosman, J. A.; Keedy, V.; Patel, M. R.; Shapiro, G. I.; Mier, J. W.; Tolcher, A. W.; Wang-Gillam, A.; Sznol, M.; Flaherty, K.; Buchbinder, E.; Carvajal, R. D.; Varghese, A. M.; Lacouture, M. E.; Ribas, A.; Patel, S. P.; DeCrescenzo, G. A.; Emery, C. M.; Groover, A. L.; Saha, S.; Varterasian, M.; Welsch, D. J.; Hyman, D. M.; Li, B. T. First-in-class erk1/2 inhibitor ulixertinib (bvd-523) in patients with mapk mutant advanced solid tumors: Results of a phase i dose-escalation and expansion study. *Cancer Discovery* **2018**, *8*, 184.

(10) Blake, J. F.; Burkard, M.; Chan, J.; Chen, H.; Chou, K.-J.; Diaz, D.; Dudley, D. A.; Gaudino, J. J.; Gould, S. E.; Grina, J.; Hunsaker, T.; Liu, L.; Martinson, M.; Moreno, D.; Mueller, L.; Orr, C.; Pacheco, P.; Qin, A.; Rasor, K.; Ren, L.; Robarge, K.; Shahidi-Latham, S.; Stults, J.; Sullivan, F.; Wang, W.; Yin, J.; Zhou, A.; Belvin, M.; Merchant, M.; Moffat, J.; Schwarz, J. B. Discovery of (s)-1-(1-(4-chloro-3-fluorophenyl)-2-hydroxyethyl)-4-(2-((1-methyl-1h-pyrazol-5-yl)-amino)pyrimidin-4-yl)pyridin-2(1h)-one (gdc-0994), an extracellular signal-regulated kinase 1/2 (erk1/2) inhibitor in early clinical development. *J. Med. Chem.* **2016**, *59*, 5650−5660.

(11) ATG-017: Safety and preliminary efficacy of atg-017 monotherapy in advanced solid tumors and hematological malignancies (eraser). https://ClinicalTrials.gov/show/NCT04305249.

(12) Ward, R. A.; Anderton, M. J.; Bethel, P.; Breed, J.; Cook, C.; Davies, E. J.; Dobson, A.; Dong, Z.; Fairley, G.; Farrington, P.; Feron, L.; Flemington, V.; Gibbons, F. D.; Graham, M. A.; Greenwood, R.; Hanson, L.; Hopcroft, P.; Howells, R.; Hudson, J.; James, M.; Jones, C. D.; Jones, C. R.; Li, Y.; Lamont, S.; Lewis, R.; Lindsay, N.; McCabe, J.; McGuire, T.; Rawlins, P.; Roberts, K.; Sandin, L.; Simpson, I.; Swallow, S.; Tang, J.; Tomkinson, G.; Tonge, M.; Wang, Z.; Zhai, B. Discovery of a potent and selective oral inhibitor of erk1/2 (azd0364) that is efficacious in both monotherapy and combination therapy in models of nonsmall cell lung cancer (nsclc). *J. Med. Chem.* **2019**, *62*, 11004−11018.

(13) Bhagwat, S. V.; McMillen, W. T.; Cai, S.; Zhao, B.; Whitesell, M.; Shen, W.; Kindler, L.; Flack, R. S.; Wu, W.; Anderson, B.; Zhai, Y.; Yuan, X.-J.; Pogue, M.; Van Horn, R. D.; Rao, X.; McCann, D.; Dropsey, A. J.; Manro, J.; Walgren, J.; Yuen, E.; Rodriguez, M. J.; Plowman, G. D.; Tiu, R. V.; Joseph, S.; Peng, S.-B. Erk inhibitor ly3214996 targets erk pathway-driven cancers: A therapeutic approach toward precision medicine. *Mol. Cancer Ther.* **2020**, *19*, 325−336.

(14) Aronchik, I.; Dai, Y.; Labenski, M.; Barnes, C.; Jones, T.; Qiao, L.; Beebe, L.; Malek, M.; Elis, W.; Shi, T.; Mavrommatis, K.; Bray, G. L.; Filvaroff, E. H. Efficacy of a covalent erk1/2 inhibitor, cc-90003, in kras-mutant cancer models reveals novel mechanisms of response and resistance. *Mol. Cancer Res.* **2019**, *17*, 642−654.

(15) Boga, S. B.; Deng, Y.; Zhu, L.; Nan, Y.; Cooper, A. B.; Shipps, G. W.; Doll, R.; Shih, N.-Y.; Zhu, H.; Sun, R.; Wang, T.; Paliwal, S.; Tsui, H.-C.; Gao, X.; Yao, X.; Desai, J.; Wang, J.; Alhassan, A. B.; Kelly, J.; Patel, M.; Muppalla, K.; Gudipati, S.; Zhang, L.-K.; Buevich, A.; Hesk, D.; Carr, D.; Dayananth, P.; Black, S.; Mei, H.; Cox, K.; Sherborne, B.; Hruza, A. W.; Xiao, L.; Jin, W.; Long, B.; Liu, G.; Taylor, S. A.; Kirschmeier, P.; Windsor, W. T.; Bishop, R.; Samatar, A. A. Mk-8353: Discovery of an orally bioavailable dual mechanism erk inhibitor for oncology. *ACS Med. Chem. Lett.* **2018**, *9*, 761−767.

(16) KO-947: First-in-human study of ko-947 in nonhematological malignancies. https://ClinicalTrials.gov/show/NCT03051035.

(17) LTT462: A phase i clinical study with the investigational compound ltt462 in adult patients with specific advanced cancers. https://ClinicalTrials.gov/show/NCT02711345.

(18) ASN007: A study of asn007 in patients with advanced solid tumors. https://ClinicalTrials.gov/show/NCT03415126.

(19) HH2710: A study to evaluate the safety, tolerability, and pharmacokinetics of hh2710 in patients with advanced tumors. https://ClinicalTrials.gov/show/NCT04198818.

(20) Morris, E. J.; Jha, S.; Restaino, C. R.; Dayananth, P.; Zhu, H.; Cooper, A.; Carr, D.; Deng, Y.; Jin, W.; Black, S.; Long, B.; Liu, J.; DiNunzio, E.; Windsor, W.; Zhang, R.; Zhao, S.; Angagaw, M. H.; Pinheiro, E. M.; Desai, J.; Xiao, L.; Shipps, G.; Hruza, A.; Wang, J.; Kelly, J.; Paliwal, S.; Gao, X.; Babu, B. S.; Zhu, L.; Daublain, P.; Zhang, L.; Lutterbach, B. A.; Pelletier, M. R.; Philippar, U.; Siliphaivanh, P.; Witter, D.; Kirschmeier, P.; Bishop, W. R.; Hicklin, D.; Gilliland, D. G.; Jayaraman, L.; Zawel, L.; Fawell, S.; Samatar, A. A. Discovery of a novel erk inhibitor with activity in models of acquired resistance to braf and mek inhibitors. *Cancer Discovery* **2013**, *3*, 742−750.

(21) Heightman, T. D.; Berdini, V.; Braithwaite, H.; Buck, I. M.; Cassidy, M.; Castro, J.; Courtin, A.; Day, J. E. H.; East, C.; Fazal, L.; Graham, B.; Griffiths-Jones, C. M.; Lyons, J. F.; Martins, V.; Muench, S.; Munck, J. M.; Norton, D.; O'Reilly, M.; Palmer, N.; Pathuri, P.; Reader, M.; Rees, D. C.; Rich, S. J.; Richardson, C.; Saini, H.; Thompson, N. T.; Wallis, N. G.; Walton, H.; Wilsher, N. E.; Woolford, A. J.-A.; Cooke, M.; Cousin, D.; Onions, S.; Shannon, J.; Watts, J.; Murray, C. W. Fragment-based discovery of a potent, orally bioavailable inhibitor that modulates the phosphorylation and catalytic activity of erk1/2. *J. Med. Chem.* **2018**, *61*, 4978−4992.

(22) Munck, J. M.; Berdini, V.; Bevan, L.; Brothwood, J. L.; Castro, J.; Courtin, A.; East, C.; Ferraldeschi, R.; Heightman, T. D.; Hindley, C. J.; Kucia-Tran, J.; Lyons, J. F.; Martins, V.; Muench, S.; Murray, C.

https://doi.org/10.1021/acs.jmedchem.1c00905
J. Med. Chem. 2021, 64, 12286−12303

W.; Norton, D.; O'Reilly, M.; Reader, M.; Rees, D. C.; Rich, S. J.; Richardson, C. J.; Shah, A. D.; Stanczuk, L.; Thompson, N. T.; Wilsher, N. E.; Woolford, A. J.-A.; Wallis, N. G. Astx029, a novel dual-mechanism erk inhibitor, modulates both the phosphorylation and catalytic activity of erk. *Mol. Cancer Ther.* **2021**, DOI: 10.1158/1535-7163.mct-20-0909.

(23) Kato, M. Intestinal first-pass metabolism of cyp3a4 substrates. *Drug Metab. Pharmacokinet.* **2008**, *23*, 87−94.

(24) Waring, M. J. Defining optimum lipophilicity and molecular weight ranges for drug candidates—molecular weight dependent lower logd limits based on permeability. *Bioorg. Med. Chem. Lett.* **2009**, *19*, 2844−2851.

(25) Lovering, F.; Bikker, J.; Humblet, C. Escape from flatland: Increasing saturation as an approach to improving clinical success. *J. Med. Chem.* **2009**, *52*, 6752−6756.

(26) Lamanna, C.; Bellini, M.; Padova, A.; Westerberg, G.; Maccari, L. Straightforward recursive partitioning model for discarding insoluble compounds in the drug discovery process. *J. Med. Chem.* **2008**, *51*, 2891−2897.

(27) Delorme, D.; Ducharme, Y.; Brideau, C.; Chan, C.-C.; Chauret, N.; Desmarais, S.; Dubé, D.; Falgueyret, J.-P.; Fortin, R.; Guay, J.; Hamel, P.; Jones, T. R.; Lépine, C.; Li, C.; McAuliffe, M.; McFarlane, C. S.; Nicoll-Griffith, D. A.; Riendeau, D.; Yergey, J. A.; Girard, Y. Dioxabicyclooctanyl Naphthalenenitriles as Nonredox 5-Lipoxygenase Inhibitors: Structure−Activity Relationship Study Directed toward the Improvement of Metabolic Stability. *J. Med. Chem.* **1996**, *39*, 3951−3970.

(28) Roberts, A. W.; Davids, M. S.; Pagel, J. M.; Kahl, B. S.; Puvvada, S. D.; Gerecitano, J. F.; Kipps, T. J.; Anderson, M. A.; Brown, J. R.; Gressick, L.; Wong, S.; Dunbar, M.; Zhu, M.; Desai, M. B.; Cerri, E.; Heitner Enschede, S.; Humerickhouse, R. A.; Wierda, W. G.; Seymour, J. F. Targeting bcl2 with venetoclax in relapsed chronic lymphocytic leukemia. *N. Engl. J. Med.* **2016**, *374*, 311−322.

(29) Smith, C. C.; Levis, M. J.; Litzow, M. R.; Perl, A. E.; Altman, J. K.; Gill, S.; Yuen, G.; Bonate, P.; Kadokura, T.; James, A. J.; Liu, C.; Nagase, I.; Fisniku, O.; Bahceci, E. Pharmacokinetics and pharmacodynamics of gilteritinib in patients with relapsed or refractory acute myeloid leukemia. *J. Clin. Oncol.* **2016**, *34*, 7026.

(30) ASTX029: Study of astx029 in subjects with advanced solid tumors. https://ClinicalTrials.gov/show/NCT03520075.

(31) Aronov, A. M.; Tang, Q.; Martinez-Botella, G.; Bemis, G. W.; Cao, J.; Chen, G.; Ewing, N. P.; Ford, P. J.; Germann, U. A.; Green, J.; Hale, M. R.; Jacobs, M.; Janetka, J. W.; Maltais, F.; Markland, W.; Namchuk, M. N.; Nanthakumar, S.; Poondru, S.; Straub, J.; ter Haar, E.; Xie, X. Structure-guided design of potent and selective pyrimidylpyrrole inhibitors of extracellular signal-regulated kinase (erk) using conformational control. *J. Med. Chem.* **2009**, *52*, 6362−6368.

(32) Squires, M. S.; Feltell, R. E.; Wallis, N. G.; Lewis, E. J.; Smith, D.-M.; Cross, D. M.; Lyons, J. F.; Thompson, N. T. Biological characterization of at7519, a small-molecule inhibitor of cyclin-dependent kinases, in human tumor cell lines. *Mol. Cancer Ther.* **2009**, *8*, 324−332.

(33) Workman, P.; Aboagye, E. O.; Balkwill, F.; Balmain, A.; Bruder, G.; Chaplin, D. J.; Double, J. A.; Everitt, J.; Farningham, D. A. H.; Glennie, M. J.; Kelland, L. R.; Robinson, V.; Stratford, I. J.; Tozer, G. M.; Watson, S.; Wedge, S. R.; Eccles, S. A. Guidelines for the welfare and use of animals in cancer research. *Br. J. Cancer* **2010**, *102*, 1555.

(34) Hollands, C. The animals (scientific procedures) act 1986. *Lancet* **1986**, *328*, 32−33.

(35) Wilkinson, G. R.; Shand, D. G. Commentary: A physiological approach to hepatic drug clearance. *Clin. Pharmacol. Ther.* **1975**, *18*, 377−390.

https://doi.org/10.1021/acs.jmedchem.1c00905
J. Med. Chem. 2021, 64, 12286−12303